Manuscript

**Online article** 

Confidential

## 1 Massively parallel quantification of CRISPR editing in cells by TRAP-seq

## 2 enables better design of Cas9, ABE, CBE gRNAs of high efficiency and accuracy

3

## 4 Authors

- 5 Xi Xiang <sup>1-4</sup>\*, Kunli Qu <sup>1, 5</sup>\*, Xue Liang <sup>1, 5</sup>\*, Xiaoguang Pan <sup>1, 5</sup>\*, Jun Wang <sup>1-3</sup>, Peng Han <sup>1,2,5</sup>,
- 6 Zhanying Dong<sup>1</sup>, Lijun Liu<sup>1,5</sup>, Jiayan Zhong<sup>6</sup>, Tao Ma<sup>6</sup>, Yiqing Wang<sup>1</sup>, Jiaying Yu<sup>1,2</sup>, Xiaoying
- 7 Zhao <sup>1,2</sup>, Siyuan Li <sup>1,2</sup>, Zhe Xu <sup>1,2</sup>, Jinbao Wang <sup>6</sup>, Xiuqing Zhang <sup>2,3</sup>, Hui Jiang <sup>6</sup>, Fengping Xu <sup>1,3</sup>,
- 8 Lijin Zou<sup>7</sup>, Huajing Teng<sup>8</sup>, Xin Liu<sup>3</sup>, Xun Xu<sup>3,9</sup>, Jian Wang<sup>3</sup>, Huanming Yang<sup>3,10</sup>, Lars Bolund
- 9 <sup>1,3,4,5</sup>, George M. Church <sup>11</sup>, Lin Lin <sup>1,4,12,‡</sup> & Yonglun Luo <sup>1,3,4,5,12,‡,#</sup>

## 10 Affiliations

- <sup>1</sup>Lars Bolund Institute of Regenerative Medicine, BGI-Qingdao, Qingdao 266555, China.
- <sup>2</sup>BGI Education Center, University of Chinese Academy of Sciences, Shenzhen 518083, China.
- 13 <sup>3</sup>BGI-Shenzhen, Shenzhen 518083, China.
- <sup>4</sup>Department of Biomedicine, Aarhus University, Aarhus 8000, Denmark.
- 15 <sup>5</sup>Qingdao-Europe Advanced Institute for Life Sciences, BGI-Shenzhen, Qingdao 266555, China
- 16 <sup>6</sup>MGI, BGI-Shenzhen, Shenzhen 518083, China.
- 17 <sup>7</sup>The First Affiliated Hospital of Nanchang University, Nanchang, Jiangxi 330006, P.R. China
- 18 <sup>8</sup>Key Laboratory of Carcinogenesis and Translational Research, Department of Radiation Oncology,
- 19 Peking University Cancer Hospital & Institute, Beijing, China
- 20 <sup>9</sup>Guangdong Provincial Key Laboratory of Genome Read and Write, BGI-Shenzhen, Shenzhen,
- 21 518120, China
- <sup>10</sup>Guangdong Provincial Academician Workstation of BGI Synthetic Genomics, BGI-Shenzhen,
- 23 Shenzhen, 518120, China
- <sup>11</sup> Department of Genetics, Blavatnik Institute, Harvard Medical School, Boston, MA 02115, USA
- <sup>12</sup> Steno Diabetes Center Aarhus, Aarhus University, Aarhus 8200, Denmark
- 26 # lead contact
- 27 \*These authors contribute equally to the study and should be regarded as co-first authors.
- 28 <sup>‡</sup>Correspondence addressed to: Lin Lin: <u>lin.lin@biomed.au.dk</u> or Yonglun Luo: <u>alun@biomed.au.dk</u>
- 29
- 30
- 31

#### Manuscript

#### Online article

#### Confidential

#### 32 Abstract

The CRISPR RNA-guided endonucleases Cas9, and Cas9-derived adenine/cytosine base editors 33 (ABE/CBE), have been used in both research and therapeutic applications. However, broader use of 34 35 this gene editing toolbox is hampered by the great variability of efficiency among different target sites. Here we present TRAP-seq, a versatile and scalable approach in which the CRISPR gRNA 36 37 expression cassette and the corresponding surrogate site are captured by Targeted Reporter Anchored Positional Sequencing in cells. TRAP-seq can faithfully recapitulate the CRISPR gene editing 38 39 outcomes introduced to the corresponding endogenous genome site and most importantly enables 40 massively parallel quantification of CRISPR gene editing in cells. We demonstrate the utility of this 41 technology for high-throughput quantification of SpCas9 editing efficiency and indel outcomes for 12,000 gRNAs in human embryonic kidney cells. Using this approach, we also showed that TRAP-42 43 seq enables high throughput quantification of both ABE and CBE efficiency at 12,000 sites in cells. This rich amount of ABE/CBE outcome data enable us to reveal several novel nucleotide features 44 (e.g. preference of flanking bases, nucleotide motifs, STOP recoding types) affecting base editing 45 efficiency, as well as designing improved machine learning-based prediction tools for designing 46 47 SpCas9, ABE and CBE gRNAs of high efficiency and accuracy (>70%). We have integrated all the 12,000 CRISPR gene editing outcomes for SpCas9, ABE and CBE into a CRISPR-centered portal: 48 49 The Human CRISPR Atlas. This study extends our knowledge on CRISPR gene and base editing, and will facilitate the application and development of CRISPR in both research and therapy. 50

51 52

53 Keywords

54 Gene editing, A-to-G base editing, C-to-T base editing, Genome engineering, System biology

55

#### Manuscript

#### Online article

#### Confidential

#### 56 INTRODUCTION

57 Clustered Regularly Interspaced Short Palindromic Repeats (CRISPR) and CRISPR-associated protein 9 (Cas9) are essential adaptive immune components in most bacteria. The system has 58 59 successfully been harnessed for programmable RNA-guided genome editing in prokaryotes, humans and many other living organisms [1-5]. The Streptococcus pyogenes Cas9 (SpCas9) is the most 60 extensively studied and broadly applied Cas9 protein, amongst other Cas9 orthologs (e.g. SaCas9, 61 StCas9, NmCas9) [6-9] and Cas proteins (e.g. Cas12a, Cas13) [10, 11]. Guided by a programmable 62 63 small RNA molecule (also known as gRNA), the SpCas9 protein introduces a double-stranded DNA 64 break (DSB) to the DNA target site, which constitutes a complementary protospacer sequences and a canonical protospacer adjacent motif (PAM) [2]. The classical CRISPR gene editing is achieved by 65 reparation of the DSBs in living organisms by the endogenous DNA repair mechanisms, 66 predominantly by the NHEJ and MMEJ pathways in mammalian cells. This process generates indels 67 (deletions or insertions) to the repaired site [12]. It is thus essential to have data from CRISPR editing 68 in cells to develop accurate prediction rule sets of CRISPR activity. 69

70

71 The simplicity of the CRISPR system, the flexibility for modifying the Cas9 protein, and the increasing efforts from CRISPR scientists and pharmaceutical companies have extensively broadened 72 73 the CRISPR-Cas9-based gene editing toolkits. We are now enabled to epigenetically perturb endogenous gene expression [13, 14], fluorescently label endogenous DNA elements [15] and site-74 75 specifically edit single nucleotides [16-20]. The CRISPR base editors, which comprise two major 76 classes: adenine base editors (ABE) and cytosine base editors (CBE), have increasingly evolved as 77 attracting tools for gene editing. These base editors are created by fusing a catalytically dead Cas9 78 (dCas9) or Cas9 nickase (nCas9) to either an adenine deaminase or a cytidine deaminase [18, 19]. 79 Without introducing double stranded DNA breaks, the ABE and CBE base editors, respectively, can 80 efficiently create an A to G (or T to C on the complementary strand) and C to T (or G to A on the 81 complementary strand) substitution within a small editing window of the target site [16, 21-23]. 82 Albeit all these fantastic developments and applications of the CRISPR-Cas9 gene editing theme, there is still an urgent need of methods and high throughput data on the Cas9-induced DBS repair 83 84 outcomes, as well as ABE and CBE efficiencies, to ensure a successful CRISPR gene editing outcome. Such cataloged data of Cas9 and base editor efficiencies will allow the selection of experimentally 85 validated gRNAs, as well as for developing better rules for in silico Cas9, ABE, and CBE gRNAs 86 87 design.

#### Manuscript

#### **Online article**

#### Confidential

#### 88

89 Quantification of gRNA activity at the endogenous sites in cells is limited by scale. In vitro 90 approaches (in a test-tube) can overcome the scale but fails to recapitulate the effects of genome and 91 epigenome architectures and cellular DNA repair mechanisms on CRISPR editing [24, 25]. Methods 92 based on integrating synthetically barcoded DNA constructions were developed for large-scale 93 measuring of Cas9-induced DSB repair outcomes of gRNAs in cells [26-28]. Currently, we lack large-scale ABE and CBE editing data for developing better rules for designing base editing gRNAs. 94 95 In this study, we developed an assay system for massively parallel quantification of a large-scale CRISPR gRNAs activities in human cells. We optimized the design and procedures for generation 96 97 and in-cell CRISPR editing of synthetically barcoded DNA constructs. Each construct contains a unique gRNA expression cassette and the corresponding surrogate target site. Using this method, 98 99 Targeted Reporter Anchored Positional Sequencing (hereafter referred as TRAP-seq), we demonstrated the applicability of TRAP-seq for massively parallel quantification of the SpCas9-100 induced DSB repair outcomes, ABE and CBE efficiency and profiles for 12,000 gRNAs in human 101 102 embryonic kidney cells.

103

104

#### Manuscript

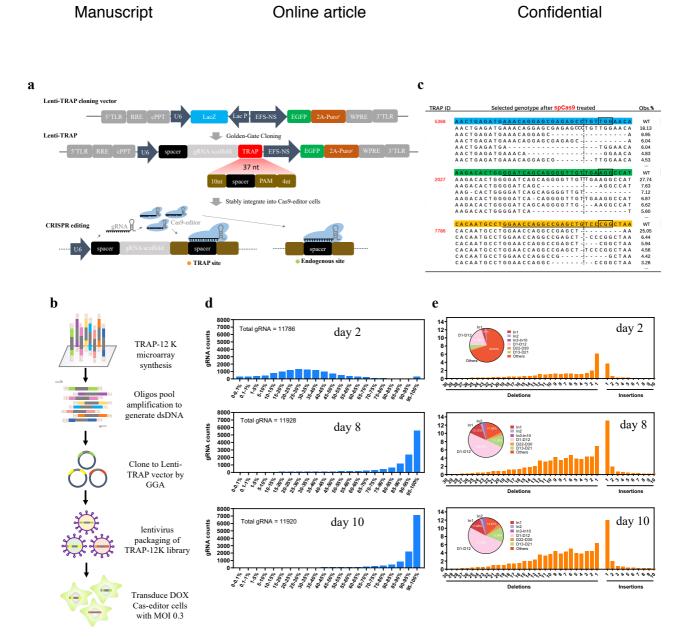
#### **Online article**

#### Confidential

#### 105 **RESULTS**

#### 106 Design and functional validation of the lentivirus-based TRAP-seq system

To streamline vector cloning, gRNA expression and delivery into cells, we firstly designed a 107 lentivirus-based system with four main features: (1) A human U6 promoter; (2) Golden-Gate 108 109 Assembly (GGA) based cloning with a lac Z marker for precise and efficient insertion of an expression cassette; (3) A green fluorescent protein (GFP) marker for measuring viral titer and real-110 time tracking of viral delivery; (4) A puromycin selection gene for enrichment of stably transduced 111 cells (Fig. 1a and S1). Essentially, this lentivirus system allows conventional GGA-based insertion 112 of a synthetic DNA containing a gRNA spacer, scaffold and the corresponding surrogate target site 113 after the U6 promoter. As current microarray-based method can only faithfully synthesize oligo pools 114 of max 170 bp, we optimized the DNA design to contain a 102bp gRNA expression cassette (20bp 115 spacer + 82bp scaffold) and a 37bp surrogate target site, flanked by a 31bp GGA cloning site and 116 PCR handles (Fig. 1a and S1). We and several other groups previously demonstrated that such a 117 surrogate target site can faithfully recapitulate the endogenous editing efficiency and indel profile [27, 118 29]. To further validate the 37 bp surrogate target site, we firstly generated HEK293T cells expressing 119 a doxycycline (Dox)-inducible SpCas9 [1], an adenine base editor (ABE7.10) [19] or a cytosine base 120 editor (CBE, BE4-Gam) [30]. Next, we performed ICE-based analysis of three different sites (AAVS1, 121 INHCB, TYMP) in the HEK293T-SpCas9, HEK293T-ABE and HEK293T-CBE cells. The results 122 validated that the CRISPR editing efficiency and outcomes from the surrogate sites were closely 123 correlated  $(r^2 = 0.96 - 0.99)$  with those from the endogenous genome sites (Fig. S2). For 124 simplification, we hereafter named the system as Targeted Reporter Anchored Positional Sequencing 125 (TRAP-seq), the 170bp synthetic oligo/DNA as TRAP oligo/DNA, and the 37bp surrogate target site 126 127 as TRAP site.



#### 128

## 129 Figure 1 High Throughput Quantification of SpCas9 efficiency in cells by TRAP-seq

- **130 a**. Schematic illustration of the TRAP-seq system. TLR, long terminal repeat; RRE, Rev Response Element; cPPT,
- 131 central polypurine tract; U6, human U6 promoter; EFS-NS, short EFS promoter derived from EF1a. Figure not drown
- to scale.
- 133 b. Schematic illustration of oligo pool synthesis, PCR amplification, gold-gate assembly, lentivirus packaging, and
- transduction of the 12K TRAP-seq library.
- 135 c. Representative quantification of top 5 indel types for 3 TRAP sites. Dash line indicates the DSB site. Results for the
- 136 12,000 TRAP sites can be found at the CRISPR atlas database.
- d. Bar plots of SpCas9 editing efficiency of all TRAP sites measured by targeted amplicon sequencing. Results are
- 138 shown for Dox-induced HEK293T-SpCas9 cells from 2, 8 and 10 days after transduction. Corresponding results for
- 139 Dox-free HEK293T-SpCas9 are shown in Fig. S10.
- e. Bar plots of indel profiles (1-20 bp deletion, 1-10 bp insertion) for all TRAP sites introduced by SpCas9 in the Dox-
- 141 induced HEK293T-SpCas9 cells from at 2, 8, and 10 days post transduction. Pie chat quantified the proportion of major
- indel groups: 1bp insertion (ins), 2bp insertion, 3-10 bp insertion, 1-12 bp deletion, 13-21bp deletion and 22-30 bp

#### Manuscript

#### **Online article**

#### Confidential

143 deletion. Other indels and wild-type reads are presented together as "others". Corresponding results for Dox-free

- 144 HEK293T-SpCas9 are shown in Fig. S11 and S12.
- 145

#### Generation of 12K TRAP-seq lentiviral library 146

We next generated a 12K TRAP-seq library comprising 12,000 TRAP oligos by microarray synthesis 147 (Fig. 1b). The library targets 3,834 human protein-coding genes (Table S1) [31]. The gRNA spacers 148 were selected from the iSTOP database [32]. Out optimized workflow (also seen in methods) for PCR 149 amplification of the 12K TRAP-seq oligos and cloning into the lentivirus-based TRAP-seq vector 150 system is illustrated in Fig. S3a. A serial of optimizations in PCR conditions, GGA reactions and 151 lentiviral packaging were carried out to avoid unspecific amplification (Fig. S3b, c), maximize 152 153 successful ligation (Fig. S4) and properly quantify viral titer by FACS (Fig. S5), respectively.

To analyze the coverage of each TRAP oligo in our 12K TRAP-seq library, as well as to assess if the 154 whole procedure of vector cloning and lentivirus packaging/transduction affected the overall TRAP 155 representation, we performed targeted amplicon sequencing of the TRAP DNA in the 12K TRAP-

157 seq oligo library, GGA plasmid DNA and wildtype HEK293T cells transduced with the 12K TRAP-

seq lentivirus with a multiplexity of infection (MOI) of 0.3. With a constant sequencing depth (> 158

159 1,000X), all 12,000 TRAP oligos were detected in the 12K TRAP-seq library and the majority of

TRAP oligos (> 90%) were evenly distributed (Fig. S6a). Most importantly, over 99% of the TRAP 160

161 oligos were present in the 12K TRAP-seq plasmids and lentivirus preparation with high correlation

of representation for each TRAP oligo ( $r^2 = 0.86-0.91$ , Fig. S6b), suggesting that our optimized PCR, 162

163 GGA, lentivirus packaging and transduction methods faithfully retained the complexity of the 12K

TRAP-seq library without causing dramatic over/under-representation of the TRAP oligos. 164

165

156

#### Quantification of SpCas9 editing at 12,000 sites by TRAP-seq 166

To demonstrate applicability of the 12K TRAP-seq lentivirus library, we firstly investigated 167 massively parallel quantification of SpCas9 editing activity at all 12,000 TRAP sites. As 168 schematically shown in Fig. S7, we transduced the Dox inducible HEK293T-SpCas9 cells with the 169 12K TRAP-seq lentivirus (MOI = 0.3 and transduction coverage = 4.690 cells per TRAP). Puromycin 170 171 selection and Dox addition started two days after transduction to achieve maximum transduction and gene editing efficiency (Fig. S8). To enable comparison and identification of CRISPR-introduced 172 173 indels, we also transduced wildtype HEK293T cells with the 12K TRAP-seq lentivirus with same MOI and transduction coverage. We harvested genomic DNA from the transduced cells at three time 174 175 points: 2, 8, and 10 days after transduction (Fig. S7 and Fig. S8). Targeted PCRs were performed

#### Manuscript

#### Online article

#### Confidential

with a pair of universal primers specifically amplifying the TRAP DNA, followed by targeted deep sequencing with a DNA Nanoball sequencing technology [33]. With a constant sequencing depth (**Fig S9**), the proportional representation of each TRAP correlated better in the Dox-free HEK293T-SpCas9 cells ( $\mathbf{r} = 0.95$ ) than that in the Dox-induced HEK293T-SpCas9 cells ( $\mathbf{R} = 0.88$ ). Similar to CRISPR knockout screening pool libraries [34, 35], our results suggested that there existed similar cell fitness-related enrichment and depletion of the gRNAs in the 12K TRAP-seq library.

182

To measure the SpCas9 editing outcome, we firstly filtered out indels commonly found in both WT 183 and SpCas9 HEK293T cells (also see methods), which were introduced by oligo synthesis or PCRs. 184 We next analyzed the editing frequency and indel profiles for all 12,000 TRAP sites (Fig. 1c, Table 185 S2, also see CRISPR Atlas below). Although the SpCas9 expression was Dox inducible, significant 186 editing efficiencies were detected for all gRNAs in the HEK293T-SpCas9 cells at 2, 8 and 10 days 187 after transduction in Dox-free medium (Fig. S10), suggesting a substantial leakiness of SpCas9 188 expression. As expected, significantly higher editing efficiencies were achieved for all 12,000 gRNAs 189 in Dox-addition HEK293T-SpCas9 cells at 8 and 10 days after transduction (Fig. 1d). These results 190 support the notion that SpCas9 expression level and cultivation time affect gene editing efficiency 191 [36]. We and others had demonstrated that the indel outcomes introduced by SpCas9 comprises 192 193 mainly small deletions and insertions [37-39]. The distribution of indel profiles (deletion of 1-30 bp and insertion of 1-10 bp) of the 12K TRAP sites were thus assessed in the transduced HEK293T-194 195 SpCas9 cells. Two days after transduction, deletion or insertion of 1 bp were the two most frequent 196 indel types in cells (Fig. 1e, S11). Following increased editing time (Dox-free groups, Fig. S10) and SpCas9 expression (Dox-induced groups, Fig. 1e), the frequency of other indel types rose 197 198 significantly and 1 bp insertion was the most dominant indel type which is in agreement with previous 199 findings (Fig. 1e, S12) [37]. With the indel outcome, we were capable of analyzing the mutation 200 consequence of all indels on protein translation. More than 70% of the total indels led to out-of-frame 201 genotypes (Fig. S13). In conclusion, we demonstrated that TRAP-seq is a simple method for 202 massively parallel quantification of gRNA editing outcomes in cells.

203

## 204 Characterization of nucleotide features affecting SpCas9 efficiency and indel outcomes

Development of more accurate rules for *in silico* CRISPR design relies heavily on datasets of gRNA activity and indel from a large number of gRNAs. The rich gRNA activity and indels profile data generated by TRAP-seq above were valuable for further improving the performance of CRISPR

#### Manuscript

#### Online article

#### Confidential

208 design. We sought to investigate if the gRNA activity and indel outcomes measured by the TRAP-209 seq can mirror previous findings about the effects of nucleotide features on CRISPR activity. Nucleotide features such as secondary structure [24] and GC content [40] of the guide sequences 210 affect CRISPR editing efficiency. We analyzed the correlation between gRNA activity and GC 211 content and secondary structure (deltaG energy) in the gRNA spacer. Our TRAP-seq results further 212 213 confirmed that the gRNA spacer GC content (Fig. 2a, S14) and secondary structure (Fig. 2b, S15) affected SpCas9 gene editing efficiency in cells. The optimal GC content and deltaG energy is [50-214 215 70%] GC and [-5; -1] KJ/mol, respectively. Consistent with the previous finding [41], our TRAP-seq results revealed that the SpCas9 disfavors motifs of "TT" and "GCC" at the N17-N20 region (Fig. 216 2c, S16). Recent reports have discovered that indel profiles for a given gRNA is predictable [27, 28]. 217 The SpCas9 predominantly generates blunt-end double-stranded DNA breaks (DSB) between the 218 N17 and N18 nucleotide preceding the protospacer adjacent motif (PAM), which are most frequently 219 repaired by the NHEJ and MMEJ pathways in mammalian cells [42]. We compared the indel profiles 220 of approximately 12,000 gRNAs revealed by TRAP-seq to the predicted indel profiles by inDelphi, 221 a machine learning program for SpCas9 indel prediction [27]. Our results show that the overall indel 222 223 profiles (in the Dox-free or Dox-induced cells at day 8 and 10) are highly correlated with the predicted ones by inDelphi (median r = 0.51-0.65, Fig. 2d and Fig. S17). Of note, the overall correlation 224 225 between the TRAP indels in transduced cell at day 2 and indel profiles predicted by inDelphi was much lower (median r = 0.31, Fig. S17), suggesting that the indel outcome also depends on the 226 227 experimental conditions (e.g. Cas9 expression level, editing time etc.).

228

229 Among all indels, the 1bp insertion between N17 and N18 was the most abundant type (Fig. 1e). 230 Previous studies had discovered that 1bp insertion is not random [27]. We therefor asked whether the nucleotides of 1bp insertion among our 12,000 TRAP sites followed the same principle. First, we 231 232 quantified the frequency of inserted adenine (A), thymine (T), cytosine (C), guanine (G) among all 1bp insertions. The results show that the 1bp insertion favor T and disfavor G (Fig. 2e). For a given 233 234 TRAP site, however, there is a strong preference of one nucleotide type (also seen the CRISPR Atlas 235 resource). Next, we divided all 12,000 TRAP sites into four groups based on the N17 or N18 236 nucleotide and quantified the frequency of inserted bases among all 1bp insertions. Our results show 237 that the N17 nucleotide strongly defines the inserted base (Fig. 2f, S18), but less extensively affected by the N18 nucleotide (Fig. S19). Lastly, we divided all the 12,000 TRAP sites into 16 groups based 238 239 on N17N18 sequence motifs and compared the indel frequency of 1bp insertion versus deletions.

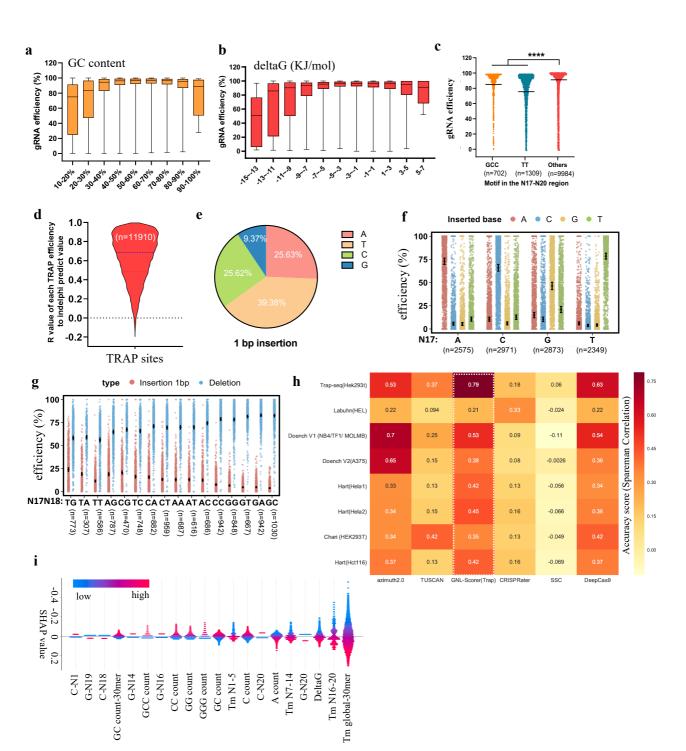
#### Manuscript

#### Online article

#### Confidential

Despite a constantly higher frequency of deletions over insertions, motifs of GN (N = A, T, C, or G) and MC (M = A or C) at N17N18 favor deletions over 1bp insertion, as compared to TN and MG motifs (**Fig. 2g, S20**). Taken together, we show that high throughput TRAP-seq enables the identification and validation of features affecting SpCas9 editing efficiency and indel outcomes. The results corroborate previous findings that SpCas9 editing outcomes are predictable in cells.

245



Manuscript

Online article

Confidential

- 247 Figure 2 Characterization of features affecting SpCas9 efficiency and indel outcomes in cells
- a. Box plot between GC content (with an interval of 10%) and SpCas9 gRNA efficiency measured in Dox-induced cells
- from Day 10. Results for other groups are shown in Fig. S14.
- **b.** Box plot between deltaG energy (with an interval of 2) and SpCas9 gRNA efficiency measured in Dox-induced cells
- from Day 10. Results for other groups are shown in Fig. S15.
- 252 c. Comparison of SpCas9 efficiency between gRNAs harboring the GCC or TT motif in N17-N20 seed region and
- 253 gRNAs without these two motifs. Data are shown for Dox-induced cells from Day 10. Results for other groups are
- shown in Fig. S16. "\*\*\*\*", p value less than 0.0001.
- d. Correlation between TRAP-seq indels and indels predicted by inDelphi from 11,910 sites. Data are shown for Dox-
- induced cells from Day 10. Results for other groups are shown in Fig. S17.
- **257** e. Pie chart of the proportion of 1bp insertion among four bases (A, T, C, G)
- **258 f**. Correlation between the inserted 1 base and the nucleotide at N17 position. Data are shown for Dox-induced cells
- from Day 10. Results for other groups are shown in Fig. S18.
- 260 g. Effects of N17N18 dinucleotide motifs on the indel frequency of 1bp insertion and deletions (1-30 bp). The gRNAs
- are divided into 16 groups based on the N17N18 motifs. For each gRNA, the total indel frequencies of 1-30bp deletionsand 1bp insertion were analyzed. "n" indicates the number of gRNAs included for each group.
- **263 h.** Comparison of SpCas9 gRNA efficacy predictions in a regression schema for various datasets and prediction models.
- i. Top 20 features that weighted the most for the GNL machine learning model. Results are shown as the SHAP
- 265 (SHapley Additive exPlanations) values. The 30mere comprises 4bp upstream, 20bp protospacer, 3 bp PAM, and 3 bp
- downstream sequences. Machine learning was based on gRNA efficiency data from Dox-induced cells at Day 10.
- 267

## 268 An improved machine learning model to predict SpCas9 efficiency

To further streamline the prediction of SpCas9 efficiency and the identification of nucleotide features 269 270 important for gRNA activity, we randomly selected 80% of the 12K TRAP-seq gRNA efficiency and trained the GNL-Scorer [43] - a machine learning algorism that we previously developed based on 271 272 the Bayesian Ridge regression (BRR) model and 2485 features. Our results showed that the GNLscorer trained with the TRAP-seq dataset (GNL-Scorer (Trap)) gave an accuracy prediction score of 273 274 over 70% (Fig. S21). To benchmark the performance of the TRAP-seq dataset and the GNL 275 prediction algorithm, we compared our dataset and GNL-Scorer (Trap) with seven previously 276 published datasets (from HEL, NB4, TF1, MOLMB, A375, Hela, HEK293T, HCT116 cells) and five 277 prediction tools (DeepCas9, Azimuth-2.0, TUSCAN, CRISPRater, SSC). Our results showed that the 278 GNL-Scorer (Trap) achieved the best accuracy score in five datasets (second best for the remaining 3 datasets) and have the best generalized prediction outcome across all test datasets (Fig. 2h). Using 279 280 the SHapley Additive exPlanations (SHAP) algorithm for explaining the feature output, our results further revealed features (such as melting temperature, GC content delta G energy, sequences motifs 281

#### Manuscript

#### Online article

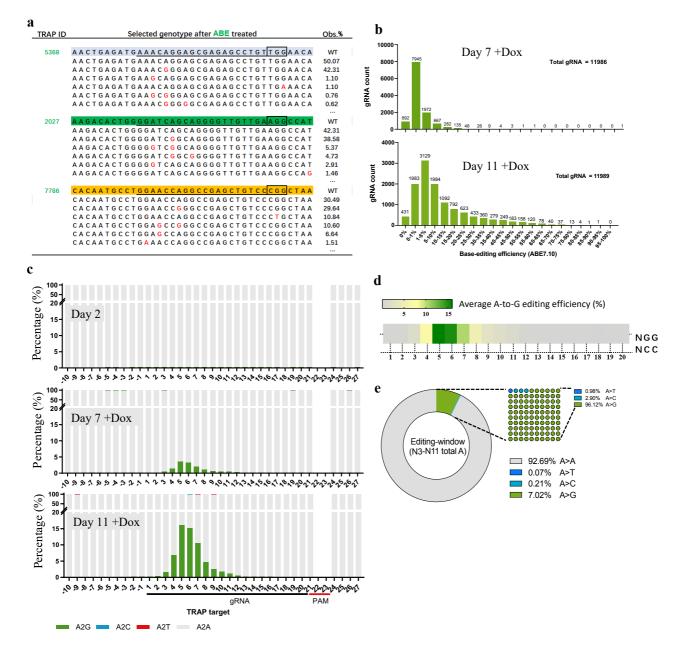
#### Confidential

etc.) that are important for the performance of our prediction model and SpCas9 efficiency (Fig. 2i).
Our results taken together suggest the TRAP-seq dataset based GNL-Scorer performs generally well
for gRNA knockout efficiency prediction that the 12K SpCas9 gRNA efficiency dataset revealed by
TRAP-seq enable better understanding of features affecting gRNA efficiency in cells, improve the
design of gRNAs of high knockout efficiency. This improved GNL-scorer algorithm for predicting
SpCas9 efficiency has been deposited to and available at public domain GitHub.

288

## 289 Quantification of CRISPR-mediated adenine base editing at 12,000 sites by TRAP-seq

Unlike SpCas9 gene editing, we still lack large-scale data of CRISPR adenine base editing (ABE) 290 efficiency. Such valuable data would enable us to develop better in silico ABE gRNA design tools. 291 Since the TRAP site could confidentially recapitulate the ABE editing outcome of the corresponding 292 endogenous site (Fig. S2), we sought to investigate the ABE editing outcomes in all 12,000 TRAP 293 sites using the 12K TRAP-seq library. Although all the 12,000 gRNAs were not specifically designed 294 for ABE editing, we reasoned that this "randomly" selected gRNA library would enable us to 295 unbiasedly identify rules affecting ABE editing efficiency. To do this, we firstly transduced 296 297 HEK293T-ABE cells with the 12K TRAP-seq lentivirus (MOI=0.3), and performed targeted amplicon sequencing of the TRAP DNAs from cells at 2, 7, and 11 days after transduction and 298 299 cultured in Dox-free or Dox-addition medium (Fig. S22). For additional controls, we also performed similar experiments with wild-type HEK293T cells, with constant transduction coverage (4,690 cells 300 per TRAP) and sequencing depth (approximately 1,000 reads per TRAP) (Fig. S23). 301



302

## 303 Figure 3 Quantification of ABE efficiency at 12,000 sites by TRAP-seq

**a.** Representation of top 5 adenine editing outcomes for three TRAP sites. Full ABE results for all 12,000 sites can befound at the CRISPR atlas resource.

306 b. Quantification of overall ABE efficiency for all gRNAs from Dox-induced HEK293T-ABE cells 7- and 11-days post
 307 transduction. Other groups are presented in Fig. S23.

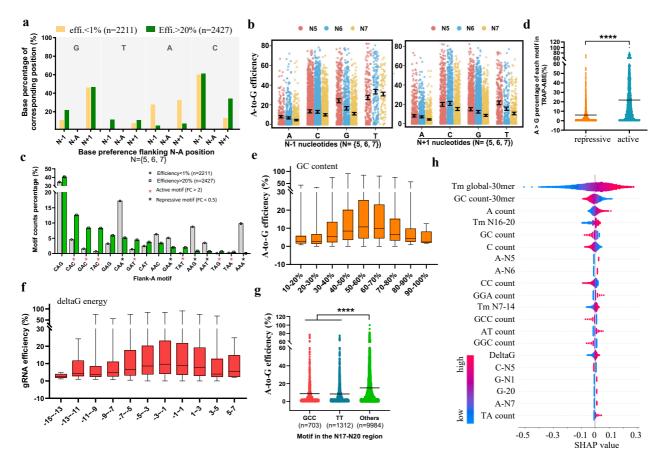
- 308 c. Quantification of overall percentage of A-to-G, A-to-T, A-to-C, and A-to-A (unedited) events across the 37bp region
- 309 of all TRAP sites. Results are from Dox-induced HEK293T-ABE cells at 2, 7- and 11-days post transduction.
- **d.** Heatmap quantification of the overall A-to-G editing efficiency within the 20nt protospacer region.
- **311** e. Summary of substitution of Adenines within the ABE editing window N3-N11.
- 312

313 Next, we quantified the edited adenine events for each 37bp TRAP site in the 12K TRAP-seq library (Fig. 3a, Table S3). Our results showed that substantial editing events (within an editing window 314 from N3 to N11) appeared 7 days after transduction in the HEK293T-ABE with Dox induction. The 315 editing efficiency increased 4-5 folds when extending the cultivation time to 11 days (Fig. 3b, S24). 316 Most importantly, the ABE editing window remained constant between N3 and N11 (Fig. 3c, S25), 317 supporting the notion that the ABE base editor is highly conserved with respect to its editing region 318 [19]. Our TRAP-seq results also validated that the highest ABE editing efficiency was observed for 319 320 adenines located at N5, N6 and N7 (Fig. 3d). Lastly, quantification of all 42,790 edited adenine sites revealed that the ABE base editor conservatively generated A-to-G substitution (96.12%), and a small 321 proportion of A-to-C (2.9%) and A-to-T (0.98%) substitutions (Fig. 3e). Although additional 322 experiments will be required to test the TRAP-seq library in more cell lines, these initial studies 323 suggest that the TRAP-seq is a highly valuable method for massively parallel quantification of 324 CRISPR adenine base editing efficiency in cells. 325

326

## 327 Characterization of nucleotide features affecting ABE efficiency

328 We also sought to characterize features that affect ABE efficiency. To enable comparisons, we first selected two groups of gRNAs based on ABE efficiency: (1) high efficiency ABE gRNAs (n = 2,331, 329 at least one edited adenine site had an efficiency over 20% with the protospacer region N1-N20) and 330 (2) low efficiency ABE gRNAs (n = 2,589, the efficiency of any edited adenine site within the 331 332 protospacer N1-N20 lower than 1%). Next, we compared the base percentage between the low and 333 high efficiency gRNAs across the 37bp TRAP region for the low and high efficiency ABE gRNAs. Not surprisingly, high efficiency gRNAs showed overrepresentation of Adenine within the editing 334 335 window N3-N7 (Fig. S26). Interestingly, high efficiency gRNAs favored Guanine over Thymine in the seed region (N17 to N20), the distal protospacer region (N-1 to N4) and the N21 base of the PAM. 336 337 The presence of Cytosine in N20 was disfavored for high efficiency gRNAs.



## 338

## 339 Figure 4 Characterization of nucleotide features affecting ABE efficiency

**340** a. Proportion of frank-A (A bases located at the core editing window N5-N7) bases (A, T, C, G) between high (edited A

- 342 N7) efficiency ABE gRNAs. Results are based on the data from the Dox-induced HEK293T-ABE cells from day 11.
- b. A-to-G editing efficiency for A bases located at N5-N7, grouped based on the flanking bases. Results are based onthe data from the Dox-induced HEK293T-ABE cells from day 11.
- **c.** Comparison of the frequency of NAN (N = A, T, C, G) trinucleotide motifs between high and low efficiency ABE
- 346 gRNAs (bold A referred to the deaminated bases within the N5-N7 core editing window). Red and black asterisks
- indicate the active and repressive motifs based on a cutoff of two-fold difference.
- 348 d. Scatter plot of edited A efficiency between sites within the active and repressive motifs. The number of "n" indicates
  349 number of sites. "\*\*\*\*", p value less than 0.0001.
- e. Box plot of overall A-to-G editing efficiency for all TRAP gRNAs according to the gRNA spacer GC content (with
- 351 10% interval). Results are based on the data from the Dox-induced HEK293T-ABE cells from day 11. Complementing
- results for other groups can be found in Fig. S26.
- **353 f.** Box plot of overall A-to-G editing efficiency for all TRAP gRNAs according to the gRNA spacer deltaG energy
- (with an interval of 2). Results are based on the data from the Dox-induced HEK293T-ABE cells from day 11.
- **355** Complementing results for other groups can be found in Fig. S27.
- **356** g. Dot plot of overall ABE efficiency between gRNAs have the GCC or TT motifs within the seed region N17-20 and
- 357 gRNAs without these two motifs. "n" indicates the number of gRNAs within each group. Results were based on the

data from the Dox-induced HEK293T-ABE cells from day 11. Complementing results for other groups can be found in
 Fig. S28. "\*\*\*\*", p value less than 0.0001.

**360 h**. Top 20 features that weighted the most based on the GNL machine learning model that affect the overall ABE

- 361 efficiency in cells. Results are shown as the SHAP (SHapley Additive exPlanations) values. The 30mere comprises 4bp
- 362 upstream, 20bp protospacer, 3 bp PAM, and 3 bp downstream sequences. Complementary SHAP results for each edited
- 363 Adenine site within the N3-N11 window were shown in Fig. S30. Results are based on the ABE editing data from the
- **364** Dox-induced HEK293T-ABE cells from day 11.
- 365

We next sought to investigate the effect of intrinsic nucleotide preference on base editing efficiency. 366 To identify the intrinsic nucleotide preference for ABE7.10, we focused on the ABE efficiency at N5, 367 N6 and N7, which were the three highest ABE sites (Fig. 3d). Using a similar strategy to enable 368 comparison, we first selected two groups of gRNAs: N5-N7 high efficiency (n = 2427, at least one 369 edited adenine site had an efficiency over 20% within the core editing window N5-N7) and N5-N7 370 low efficiency (n = 2211, the efficiency of any edited adenine site within core editing window N5-371 N7 was lower than 1%). Next, we analyzed the preference of flanking bases (A, T, C, G) at N5-N7 372 for the low and high efficiency gRNAs. Our results revealed that the high efficiency ABE gRNAs 373 374 favored upstream keto (K) bases (G, T) and downstream pyrimidine (Y) bases (T, C) (Fig. 4a). The 375 presence of flanking adenine was strikingly overrepresented in the low efficiency ABE gRNAs (Fig. 4a). To validate this observation, we analyze the correlation between A-to-G editing efficiency of all 376 377 12,000 TRAP sites in N5-N7 and their flanking bases. Consistent with the previous finding, the average ABE editing efficiency is higher if the edited adenine is flanked by Keto bases upstream and 378 379 pyrimidine bases downstream (Fig. 4b), as compared to edited sites flanked by amino bases (A, C) upstream and purine bases (A, G) downstream. The overall ABE efficiency is much lower (approx. 380 381 2 to 7 folds) if the flanked base is adenine. Based on these observations, we further compared the frequency of tri-nucleotide flank-A motifs between the low and high ABE efficiency gRNAs. Using 382 a cutoff of two folds, we categorized seven (BAC, KAT, TAR) and five (AAD, SAA) motifs (bold A 383 refers to the deaminated adenine) as active and repressive flank-A motifs, respectively (Fig. 4c). To 384 further validate that, we assessed A-to-G editing efficiency between all active or repressive flank-A 385 motifs within our 12K TRAP sites. Our results showed that the A-to-G editing efficiency is 386 387 significantly higher (p < 0.0001, fold change = 4) in the active motifs as compared to the repressive 388 ones (Fig. 4d, S27).

389

Online article

390 Since the ABE editor shares principles of gRNA-guided DNA binding with SpCas9 nickase, we reasoned that many of the features (such as GC content, gRNA secondary structure (deltaG energy), 391 N17-N20 motifs) that were known to influence SpCas9 editing efficiency should also affect ABE 392 393 efficiency. To address that, we performed Pearson correlation analysis between the ABE efficiency and GC content and the deltaG energy of the guide sequence. Our results demonstrated that both GC 394 395 content (Fig. 4e, S28) and secondary structure affect ABE efficiency (Fig. 4f, S29). We also investigated and validated that the presence of TT and GCC motifs at the N17-N20 seed region 396 397 negatively affects ABE efficiency (Fig. 4e, S30).

398

## 399 An improved machine learning model to predict ABE efficiency

400 We sought to apply our GNL-scorer machine learning model [43] to systematically identify features of importance for ABE efficiency (GNL-scorer ABE) and ABE efficiency prediction rules, as well 401 as developed a new machine learning-based tool for predicting ABE efficiency. We randomly 402 selected 80% (the remaining 20% used for model evaluation) of the ABE efficiency data and trained 403 the Bayesian Ridge regression (BRR)-based GNL-scorer model with 2485 features (Fig. S31a). The 404 405 ABE efficiency prediction was performed for both A-to-G edited site efficiency in N3-N11 and the 406 overall ABE efficiency. Our results showed that the accuracy of predicting ABE is above 60% for 407 the core ABE editing window (Fig. S31b), and the accuracy of predicting the over ABE efficiency is approximately 70% (Fig. S21). The SHAP algorithm-based feature outputs further demonstrated that 408 409 our machine learning results consistently revealed that features such as the global melting temperature, 410 GC content, deltaG energy, and nucleotide compositions (such as the presence of Adenine in N5-N7, Guanine in N20) greatly affect the ABE efficiency (Fig. 4f and S32). Collectively, we demonstrate 411 412 that the rich ABE editing efficiency data revealed by TRAP-seq enable us to systematically define 413 factors influencing ABE efficiency and improve ABE gRNA design for future studies.

414

## 415 Quantification of CBE-mediated recoding efficiency at 11,979 sites by TRAP-seq

416 After demonstrating that the TRAP-seq method is versatile for massively parallel quantification of 417 SpCas9 and ABE efficiency, we sought to test the performance of TRAP-seq for high throughput 418 quantification of CBE efficiency. As mentioned earlier, all the gRNA spacers of our 12K TRAP-seq 419 library were retrieved from the iSTOP database. This allows us to address the STOP recoding 420 efficiency of all 11,979 gRNA and 3,832 genes by CBE in cells (**Fig. 5a**). First, based the optimized 421 and constant conditions of lentivirus library transduction, we performed 10 parallel TRAP-seq-library

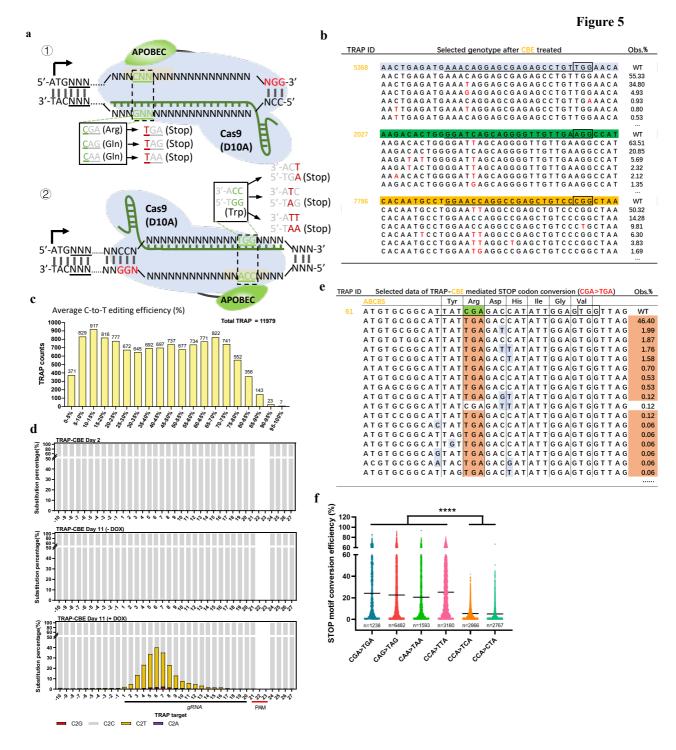
Online article

422 based CRISPR CBE editing experiments in the Dox-inducible HEK293T-CBE cells (Fig. S33). 423 Constant sequencing depths (1,000X coverage) and TRAP representation ( $\mathbf{r} = 0.96-0.97$ ) were achieved for Dox-free and Dox-addition HEK293T-CBE cells 2 and 11 days after transduction by 424 425 targeted amplicon sequencing of the TRAP region (Fig. S34). Next, to assess CBE editing, we quantified the efficiency of C-to-T edit, as well as C-to-G and C-to-A edits, of all C bases within the 426 427 37bp of all 11,979 TRAP sites (Fig. 5b, Table S4, full results were shown in the CRISPR Atlas database). As seen from the overall (Fig. 5c, S35) and C-to-T site (Fig. 5d) CBE efficiency plots, 428 429 quantification of the average efficiency of all edited Cs for the 11979 gRNAs revealed that there was an even distribution of gRNAs editing efficiency from 5% to 75%. There were 371 gRNAs with very 430 low CBE efficiency (0-5%) (Fig. 5c). The C-to-T CBE efficiency was primarily detected in the Dox-431 induced HEK293T-CBE cells at 11 days after transduction, indicating there was very minor leakiness 432 of CBE editor expression (Fig. 5c, S35). Of particular note, compared to ABE, the editing window 433 of CBE was broader (N1 to N16) but the highest cytosine editing efficiency was similarly found at 434 N6 (Fig. 5d, S36a). Quantification of all edited Cs revealed that the majority (93.18%) were C-to-T 435 edits, however, low frequency of unspecific C-to-G (4.54%) and C-to-A (2.27%) edits were also 436 437 observed for the CBE (BE4-gam) base editor (Fig. S36b).

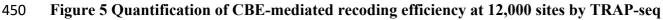
438

439 We next investigated the stop-codon recoding efficiency by CBE in cells. With the current setups in HEK293T-CBE cells, the median STOP efficiency of all 11,979 gRNA was approximately 22% (Fig. 440 441 5e, S37, S38a). A total of 3,481 genes (90%) were successfully knocked out by stop-codon recoding 442 with CBE (Fig. 38b). We also sought to analyze the efficiency of the 6 types of recoding into stop 443 codons (Fig. 5a). As seen in Fig. 5f, the recoding efficiencies of CCA-to-CTA, CCA-to-TCA and 444 CCA-to-TTA were significantly higher (p value < 0.0001) than CGA-to-TGA, CAG-to-TAG and 445 CAA-to-TAA (bold C refers to the deaminated cytosines). Taken together, we here demonstrated that 446 the TRAP-seq technology enables massively parallel quantification of CBE-mediated recoding 447 capacity in cells.

448







**<sup>451</sup> a.** Schematic illustration of the 6 stop-codon recoding schemes by CBE. Cas9 (D10A) is the Cas9 nickase used in the

- 452 testing CBE editor. The stop-codon recoding scheme is draw based on sense and anti-sense strands. "ATG", translation453 start site; "NGG", PAM of SpCas9.
- 454 **b.** Representation of top 5 cytosine base editing outcomes for three TRAP sites. Full CBE frequency results can be
- 455 found in the CRISPR Atlas database.

- 456 c. Quantification of overall CBE efficiency for all gRNAs in Dox-induced HEK293T-CBE cells at 11 days. Other
- 457 groups are presented in Fig. S33.
- 458 d. Quantification of overall percentage of C-to-T, C-to-G, C-to-A, and C-to-C (unedited) events across the 37bp region
- 459 of all TRAP sites. Results are based on HEK293T-CBE cells from 2 days post transduction, and transduced HEK293T-
- 460 CBE cells from 11 days cultured in Dox-free or Dox-addition medium.
- 461 e. Representation of CBE-mediated recoding efficiency at one TRAP site measured by TRAP-seq. Complementary
- 462 results referred to Fig. S35 and CRISPR atlas database.
- 463 f. Comparison of C-to-T efficiency between sites within the 6 stop-codon recoding types. "n" indicates the number of
- sites within each group. "\*\*\*\*", p value less than 0.0001.
- 465

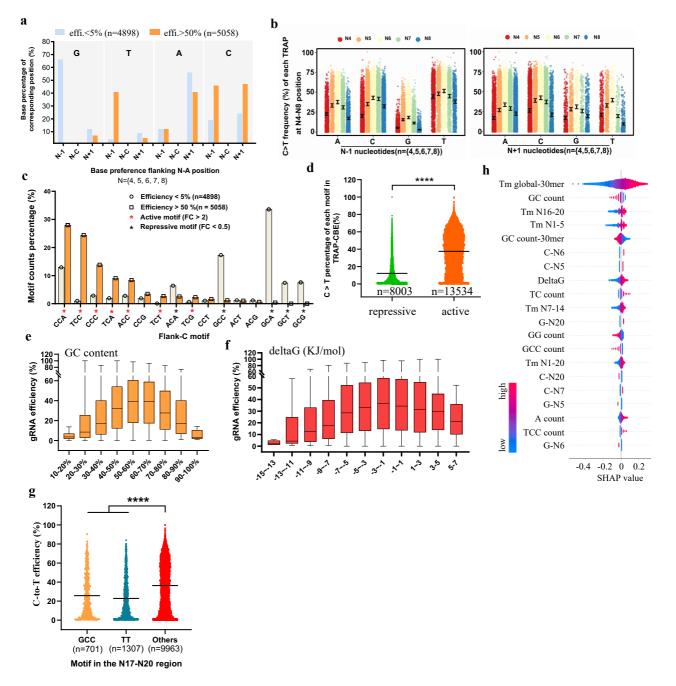
## 466 Characterization of nucleotide features affecting CBE efficiency

467 The large-scale CBE efficiency data from 56,887 edited Cs and 11,979 gRNAs enable us to characterize the features that affect CBE efficiency in cells. To simplify the analysis and 468 469 characterization, we first selected two opposing types of CBE gRNAs based on their efficiencies: low efficiency (n = 1,844, the efficiency of any edited C within the protospacer is < 5%) and high 470 471 efficiency (n = 1,731, At least one edited C efficiency within the protospacer is > 60%). Next, we compared the base preference across the 37bp TRAP regions between the two types of gRNAs. Our 472 473 results clearly show that the high efficiency CBE gRNAs favor the presence of Cytosine (N4-N8), 474 but disfavor Guanine (N3-N7) and Adenine (N5-N6) within the core editing window (Fig. S39). The 475 presence of Thymine within the seed region (N8-N20) of protospacers was underrepresented in the 476 high efficiency CBE gRNAs, which was in contrast to the N3-N6 region. Similar to our findings in ABE, high efficiency CBE gRNAs favor the presence of Guanine at proximal PAM region (N19-477 N21) and disfavored Cytosine at N20. 478

479

Since the core editing window of CBE is N4-N8 (Fig. S36), we focused on the deaminated Cytosines 480 481 within N4-N8 when further analyzing the effect of flanking bases on CBE efficiency. To enable comparison, we selected C-to-T edited sites of low (< 5%, N = 4,898) and high (> 50%, N = 5,058) 482 efficiency within the N4-N8 region. Our results show that the presence of Thymine upstream is 483 strikingly overrepresented in the highly efficient C-to-T editing, whereas the presence of Guanine 484 485 upstream is only present in the low efficiency CBE sites (Fig. 6a). In addition, the highly efficient 486 CBE sites are less frequently flanked by Adenine downstream and more frequently flanked by Cytosine, as compared to low efficiency CBE sites (Fig. 6a). To validate this observation, we 487 488 calculated the C-to-T editing efficiency at N4-N8 for all 12,000 TRAP sites. Consistent with previous 489 observations, the overall efficiency of CBE sites flanked by Thymine upstream is approximately two-

fold higher than with other flanking bases. Of note, sites flanked by Guanine upstream (as well as
downstream, but to less extent) show much lower CBE efficiency (fold changes = 2 - 12 folds) (Fig.
6b). This provides highly valuable knowledge for designing CBE gRNAs with better editing outcome.



493

## 494 Figure 6 Characterization of nucleotide features affecting CBE efficiency in cells by TRAP-

495 seq

**496 a.** Proportion of frank-C (N4-N8) bases (A, T, C, G) between high (at least one edited C base within N4-N8 was >50%

497 edited) and low (edited C efficiency for any C base within N4-N8 was less than 1%) efficiency CBE gRNAs. Results

are based on the data from the Dox-induced HEK293T-CBE cells from day 11.

499 b. C-to-T editing efficiency for C bases located at N4-N8, grouped based on the flanking bases. Results are based on the 500 data from the Dox-induced HEK293T-CBE cells from day 11.

- 501 c. Comparison of the presence of the 16 NCN trinucleotide motifs between high and low efficiency CBE gRNAs (bold
- 502 C referred to the deaminated cytosine within the N4-N8 core editing window). Red and black asterisks indicate the

503 active and repressive motifs based on a cutoff of two-fold difference.

- 504 d. Scatter plot of edited C efficiency between sites within the active and repressive motifs. The number of "n" indicates 505 number of sites. "\*\*\*\*", p value less than 0.0001.
- 506 e. Box plot of overall C-to-T editing efficiency for all TRAP gRNAs according to the gRNA spacer GC content (with
- 507 10% interval). Results are based on the data from the Dox-induced HEK293T-CBE cells from day 11. Complementing 508 results for other groups can be found in Fig. S36.

509 f. Box plot of overall C-to-T editing efficiency for all TRAP gRNAs according to the gRNA spacer deltaG energy

- 510 (with an interval of 2). Results are based on the data from the Dox-induced HEK293T-CBE cells from day 11.
- 511 Complementing results for other groups can be found in Fig. S38.
- 512 g. Scatter plot of overall CBE efficiency between gRNAs have the GCC or TT motifs within the seed region N17-20
- 513 and gRNAs without these two motifs. "n" indicates the number of gRNAs within each group. Results were based on the
- 514 data from the Dox-induced HEK293T-CBE cells from day 11. Complementing results for other groups can be found in 515
- Fig. S41.
- 516 h. Top 20 features that weighted the most based on the GNL machine learning model, which affect the overall CBE
- 517 efficiency in cells. Results are shown as the SHAP (SHapley Additive exPlanations) values. The 30mere comprises 4bp
- 518 upstream, 20bp protospacer, 3 bp PAM, and 3 bp downstream sequences. Complementary SHAP results for each edited
- 519 cytosine site within the protospacer N1-N20 were shown in Fig. S42. Results are based on the CBE editing data from
- 520 the Dox-induced HEK293T-CBE cells from day 11.
- 521
- Since the flanking bases played an important role on CBE efficiency, we reasoned that there exists a 522 preference of tri-nucleotide flank-C motifs (NCN; N=A, T, C, G; bold C refers to the deaminated 523 524 cytosine located at N4, N5, N6, N7 or N8) for active or repressive CBE. To identify these motifs, we compared the frequency of all 16 NCN motifs between the low (N=4898, efficiency < 5%) and high 525 (N=5058, efficiency > 50%) efficiency cytosine editing sites in N4-N8. Based on a two-fold 526 difference, we identified seven (TCN, CCM and ACC; N=A, T, C, G; M = A, C) and five (ACA and 527 GCN) as active and repressive motifs, respectively (Fig. 6c). To validate this, we further compared 528 529 the C-to-T editing efficiency between the active and repressive motifs for all 21537 edited C sites in our 12K TRAP-seq library. The C-to-T editing efficiency of the active motifs were significantly 530 531 higher (fold change = 3, p < 0.0001) than those within the repressive motifs (Fig. 6d, S40). We also sought to investigate if the CBE efficiency shared features with SpCas9 editing efficiency using our 532 533 CBE 12K TRAP-seq data. Thus, we analyzed the correlation between CBE efficiency and the GC content, the gRNA spacer secondary structure, as well as the proximal PAM motifs. Our results show 534

- that, similar to SpCas9 and ABE, the CBE efficiency is affected by the gRNA spacer GC content
- 536 (Fig. 6e, S41) and secondary structure (Fig. 6f, S42). The CBE efficiency of gRNAs is significantly
- 537 (p < 0.0001) lower with TT or GGC motifs at the proximal (17-N20) PAM region (Fig. 6g, S43).
- 538

# 539 An improved machine learning model to predict CBE efficiency

540 We further took advantage of our GNL-scorer machine learning model to development a prediction tool and systematically evaluate the effect of 2485 features on CBE efficiency. Based on randomly 541 542 selecting 80% of 12K gRNAs CBE efficiency for model training and 20% for model evaluation, our results showed that the accuracy prediction score of CBE efficiency by the GNL machine learning 543 544 model reaches approximately 80% (Fig. S21). Apart from predicting the overall CBE efficiency, our machine learning-based prediction tool provides highly precise predicting outcome of the site-545 specific CBE efficiency within the editing window (Fig. S44). Consistently, our machine learning 546 results further showed that features such as melting temperatures, GC content, deltaG energy, 547 nucleotide composition (e.g. the presence of cytosine at N5-N7, nucleotide counts, motifs) greatly 548 affect CBE efficiency (Fig. 6h and Fig S45). Finally, the machine learning-based CBE efficiency 549 prediction algorism (GNL-scorer CBE) has also been deposited to the GitHub to facilitate the design 550 551 of CBE gRNAs of high efficiency. Taken together, we hereby demonstrate that high-throughput quantification of CBE efficiency by TRAP-seq enables the better understanding and design of highly 552 553 efficient CBE gRNAs in cells.

554

## 555 The CRISPR Atlas

As part of this work, a human CRISPR atlas database (http://www.crispratlas.com/crispr) has been 556 557 launched to present and integrate all the SpCas9, ABE and CBE efficiency and editing outcomes for 12,000 gRNAs in HEK293T cells. This CRISPR atlas is presented with a gene-centered and gRNA-558 559 centered summary of the overall efficiency of gRNAs and editing outcomes. For SpCas9, total 560 efficiency, indel (1-30bp deletions, 1-10bp insertions) profiles were presented for each gRNA. For 561 ABE and CBE, the overall gRNA efficiency and graphical presentation of base substitution efficiency 562 across the 37bp TRAP region were shown for all 12,000 TRAP sites. We believe that the CRISPR atlas database generated by this study will complement the existing CRISPR resources in gRNA 563 design [44], efficiency prediction [45, 46] and indel prediction [27], thus streamlining the application 564 of CRISPR in functional studies. 565

566

Online article

Confidential

#### 567 **DISCUSSION**

In conclusion, the work described here demonstrates the broad applicability of the TRAP-seq system 568 for massively parallel quantification of SpCas9, ABE and CBE efficiency in human cells. Recent 569 570 studies published by other groups have demonstrated that the surrogate target sites can well mimic the SpCas9 indel outcomes at the corresponding endogenous sites, and thus predict the SpCas9 indel 571 572 profile for a given gRNA in cells [26, 28, 40]. Consistent with that, we demonstrate corroborating findings with our TRAP-seq method and further expand the data of SpCas9 knockout efficiency and 573 574 indel profiles with 12,000 gRNAs. This will aid the improvement of CRISPR gRNA design for gene knockout purposes with machine learning models [40, 45]. With such a large amount of SpCas9 575 576 efficiency data, it is possible to systematically identify both previously known as well as novel features that affect CRISPR gene editing efficiency. Importantly, according to our knowledge, this is 577 578 the first time that both ABE and CBE efficiencies are measured at such a large scale in cells. Based on the 12K ABE and CBE TRAP-seq data, our analyses identify several novel features (such as the 579 580 preference of flanking bases, active/repressive tri-nucleotide motifs) that strongly influence ABE and CBE efficiency in cells, respectively. We believe that incorporating the nucleotide features of 581 582 importance for ABE and CBE efficiency from this study will improve the performance of in silico 583 base editing designers such as BE-Designer [47] and Beditor [48]. However, we acknowledge that 584 there might be a difference in the DNA repair machinery between different cell types and organisms, which will potentially affect the SpCas9, ABE and CBE efficiency and outcome. Additional 585 586 experiments will be required to test the SpCas9, ABE and CBE efficiency with TRAP-seq in more 587 cell lines in the future.

588

589 The concept of using surrogate target sites to capture the gene editing outcomes is highly attractive. 590 We and other groups have generated dual-fluorescence-based surrogate systems for rapid evaluation 591 of ZFNs, TALENs and CRISPR-Cas9 activity in cells [29, 49, 50]. The DSBs generated by CRISPR-592 Cas9 were predominantly repaired by the NHEJ and MMEJ pathways, which will lead to the 593 introduction of small indels at the DBS site. However, large deletions or chromosomal 594 rearrangements have also been reported in CRISPR editing as outcomes of repaired mediated by e.g. 595 HDR or SSA in cells [51, 52]. The TRAP-seq system developed in this study is based on a 37bp surrogate target site. Thus, SpCas9 editing outcomes such as large deletions or chromosomal 596 arrangements will not be captured by our method. However, for ABE and CBE, the editing outcomes 597 598 would not be affected by such a size-related problem.

Online article

599

Earlier, we have discovered that chromatin accessibility at the editing sites affect CRISPR gene editing efficiency [24]. Since the TRAP-seq library were randomly inserted in the genome of the targeted cells, the chromatin accessibility state of the surrogate site might be different from the endogenous target site. It would be interesting to apply the TRAP-seq system to systematically analyze the epigenetic factors (e.g. DNA methylation, chromatic accessibility) on ABE, CBE efficiency in future studies.

606

In this study, we demonstrate the TRAP-seq system with applications in massively parallel 607 quantification of editing efficiency for SpCas9 and base editors (ABE and CBE) derived from the 608 SpCas9. The current CRISPR-based gene editing toolbox has been greatly expanded with the 609 610 engineered SpCas9 (e.g. xCas9, eSpCas9, SpCas9-HF1), the SpCas9 orthologs (e.g. SaCas9, StCas9, NmCas9) and other Cas proteins (e.g. Cas12a) [53-55]. However, features affecting the editing 611 efficiency and indel outcomes are still rarely explored for most of these Cas proteins, which will limit 612 the applications of this great toolbox. We believe that the TRAP-seq will become an important 613 614 technology for the whole CRISPR gene editing society to better understand how CRISPR gene editing works in cells. The CRISPR atlas database generated by this study will become a CRISPR-centered 615 portal, in which we provide experimentally validated gRNAs for CRISPR gene editing. Taken 616 together, the TRAP-seq technology, the SpCas9/ABE/CBE efficiency of 12,000 gRNAs, and the 617 618 CRISPR atlas database will enable us to better functionally understand how CRISPR works in cells 619 and improve CRISPR in both research, therapeutic and drug discovery applications.

620

621

## 622 MATERIALs and METHODS

#### 623 Vector construction

The empty pLenti-TRAP-seq vector backbone (shown in Fig. S1) was generated by a serial of cloning. 624 625 Briefly, we replaced the SpCas9 open reading frame (ORF) in pLentiCRISPRv2-puro (Addgene plasmid # 98290) plasmid with an enhance green fluorescence protein (EGFP) ORF based on XbaI 626 627 and BmHI digestion and T4 ligation. Next, we replaced the gRNA cassette in the EGFP-inserted pLentiCRISPRv2-puro with a synthetic Golden-Gate Assembly cassette, and hence generated a 628 629 lentivirus-based vector (hereafter referred as pLenti-TRAP-seq) allowing the insertion of TRAP DNA to the Golden-Gate cloning site by GGA. The full sequencing of the pLenti-TRAP-seq vector can be 630 downloaded from our CRISPR atlas database (www.crispratlas.com/crispr). Original plasmid stock 631 can be acquired from the corresponding authors' lab. 632

633

The doxycycline inducible SpCas9, ABE, and CBE vectors were generated by subcloning. Briefly, 634 based on a PiggyBac transposon system (full GenBank vector sequences can be found at the CRISPR 635 atlas website), which consists of an all-in-one expression system: (1) An expression cassette of a TRE 636 637 promote-driven protein expression cassette with multiple cloning sites (MCS). (2) An expression cassette of a consecutive promoter-driven Tetracycline-Controlled Transcriptional Activation and 638 639 hygromycin. The coding sequences of SpCas9 (Addgene plasmid ID # 41815), ABE 7.10 (Addgene plasmid ID # 102919), and CBE (Addgene plasmid ID # 100806) were PCR amplified and inserted 640 641 to the MCS of the PiggyBac transposon system. All vectors were validated by Sanger sequencing.

642

## 643 TRAP 12K oligos design and microarray synthesis.

A typical TRAP oligo consists of the BsmBI recognition site "**cgtete**" with 4 bp specific nucleotides "acca" upstream, following the GGA cloning linker "aCACC", one bp "g" for initiating transcription, then the 20 bp gRNA sequences of "gN20", 82bp gRNA scaffold sequence, 37 bp surrogate target sequences (10bp upstream sequences, 23 bp protospacer and PAM sequences, 4 bp downstream sequence), the downstream linker "GTTTg" and another BsmBI binding site and its downstream flanking sequences "acgg". An example of the typical TRAP oligo sequence was shown below:

- 650 "accacgteteaCACCgGTCCCCTCCACCCCACAGTGGTTTTAGAGCTAGAAATAGCAAGTTA
- 651 AAATAAGGCTAGTCCGTTATCAACTTGAAAAAGTGGCACCGAGTCGGTGCTTTTTACT
- 652 <u>TTTATCTGTCCCCTCCACCCCACAGTGGGGCCACGTTTggagacgacgg</u>". Sequences in the

black frame is the 20 bp gRNA spacer. The underline sequence is the 37 bp surrogate target site,which is termed as "TRAP target" shortly in this study.

655

656 For the 12K TRAP oligo design, we used bioinformatic tools to automatically generate the 12K TRAP oligo pools. Briefly, 1) we selected approximately 7,000 genes from the a drugable gene database 657 658 (http://dgidb.org); 2) Discard all the exons which the DNA length was less than 23 bp with filtering; 3) Select the first three coding exons of each gene. If the exons number is less than 3, keep all the 659 660 exons; 4) Extract all the possible gRNA sequences (including the PAM sequence "NGG") in these filtered exons sequence, analyzes and predictd the off-target sites of each gRNA using FlashFry 661 version 1.80 (https://github.com/mckennalab/FlashFry), discarded gRNAs with potential off-target 662 of 0-3 bp mismatches in human genome; 5) Rank each gRNA based on the number of off-target site 663 664 in an ascending order; 6) Map and extract the 10 bp upstream and 4 bp downstream flanking sequence of each selected gRNA, construct the TRAP target sequence as 10 bp upstream + 23 bp gRNA 665 (include PAM) + 4 bp downstream = 37 bp; 7) Filter out TRAPs with BsmBI recognition site, because 666 of GGA cloning; 8) Compared all the selected gRNAs with the database of CRISPR-iSTOP [56]; 9) 667 Construct the full length sequence of each TRAP, which is 170 bp; In total, the first 12K TRAP-seq 668 669 oligos contain 3832 genes and 12000 TRAPs were contained in the final TRAP-library. The 12K 670 oligo pools was synthesized in Genscript® (Nanjing, China).

671

## 672 TRAP-12K plasmid library preparation

First, the TRAP 12K oligos were cleaved and harvested from the microarray and diluted to 1 ng/ $\mu$ L. Next, we performed PCR amplifications using the primers: TRAP-oligo (BsmBI GGA)-F: 5'-TACAGCTaccacgtctcaCACC-3'; TRAP-oligo (BsmBI GGA)-R: 5'-AGCACAAccgtcgtctccAAAC-3'.

677

The PCR reaction was carried out using PrimeSTAR HS DNA Polymerase (Takara, Japan) following the manufacturer's instruction. Briefly, each PCR reaction contained 1  $\mu$ L oligo template, 0.2  $\mu$ L PrimeSTAR polymerase, 1.6  $\mu$ L dNTP mixture, 4  $\mu$ L PrimeSTAR buffer, 1  $\mu$ L forward primer (10 uM) and 1  $\mu$ L reverse primer (10 uM) and ddH2O to a final volume of 20  $\mu$ L.

682

The thermocycle program was 98°C 2min, (98°C/10s, 55°C\*/10s, 72°C/30s) with 21 cycles, then
72°C for 7min and 4°C hold. To avoid amplification bias of oligos introduced by PCR, we conducted

gradient thermocycles and performed PCR products gray-intensity analysis to determine the optimal PCR cycles of 21. The best thermocycles should be in the middle of an amplification curve. In this study, the *PCR cycles* was 21 for oligos amplification. But for PCR amplification of TRAP from cells integrated with TRAP lentivirus, the *PCR cycle* was 25. The final TRAP PCR product length was 184 bp. We performed **72** × parallel PCR reactions for 12K oligos amplification, then these PCR products were pooled and gel purified by 2% agarose gel. 1  $\mu$ g purified PCR product were quantified with PCR-free next generation sequencing (MGI Tech).

692

693 The PCR products of TRAP oligos were then used for Golden Gate Assembly (GGA) to generate the 694 TRAP 12K plasmids library. For each GGA reaction, the reaction mixture contained 100 ng pLenti-695 TRAP-seq vector, 10 ng purified 12K TRAP oligos-PCR products, 1  $\mu$ L T4 ligase (NEB), 2  $\mu$ L T4 696 ligase buffer (NEB), 1  $\mu$ L BsmBI restriction enzyme (ThermoFisher Scientific, FastDigestion) and 697 ddH2O to a final volume of 20  $\mu$ L. The GGA reactions were performed at 37°C 5 min and 22°C 10 698 min for 10 cycles, then 37°C 30 min and 75°C 15 min. **36** × parallel GGA reactions were performed 699 and the ligation products were pooled into one tube.

700

701 Transformation was then carried out using home-made chemically competent DH5a cells. For each reaction, 10 µL GGA ligation product was transformed in to 50 µL competent cells and all the 702 703 transformed cells were spread on one LB plate (15 cm dish in diameter) with Xgal, IPTG and Amp 704 selection. High ligation efficiency was determined by the presence of very few blue colonies (also 705 see Fig. S4). To ensure that there is sufficient coverage of each TRAP in the 12K TRAP-seq library, 706  $42 \times$  parallel transformations were performed and all the bacterial colonies were scraped off and 707 pooled together for plasmids midi-prep. For NGS-based quality quantification of TRAP coverage, midi-prep plasmids were used as DNA templates for TRAP PCR amplifications, followed by gel 708 709 purification and NGS sequencing.

710

## 711 TRAP-12K lentivirus packaging.

HEK293T cells were used for lentivirus package. All the cells were cultured in Dulbecco's modified
Eagle's medium (DMEM) (LONZA) supplemented with 10 % fetal bovine serum (FBS) (Gibco), 1%
GlutaMAX (Gibco), and penicillin/streptomycin (100 units penicillin and 0.1 mg streptomycin/mL)
(The culture medium was named as D10 shortly) in a 37 °C incubator with 5% CO2 atmosphere and

maximum humidity. Cells were passaged every 2-3 days when the confluence was approximately 80-90%.

718

For lentivirus packaging: Day 1: Wild-type HEK293T cells were seeded to a 10 cm culture dish,  $4 \times$ 719 720 10<sup>6</sup> cells per dish (10 dishes in total); **Day 2**: Transfection. Briefly, we refreshed the medium with 7 mL fresh culture medium to 1 hour before transfection (be gently, as the HEK293T cells are easy to 721 722 be detached from the bottom of dish); Next, we performed transfection with the PEI 40000 723 transfection method. For 10 cm dish transfection, the DNA/PEI mixture contains 13 µg pLenti-724 TRAPseq 12K vectors, 3 µg pRSV-REV, 3.75 µg pMD.2G, 13 µg pMDGP-Lg/p-RRE, 100 µL PEI 40000 solution (1  $\mu$ g/ $\mu$ L in sterilized ddH2O) and supplemented by serum-free opti MEM without 725 726 phenol red (Invitrogen) to a final volume of 1 mL. The transfection mixture was pipetted up and down 727 several times gently, then kept at room temperature (RT) for 20 min, then added into cells in a 728 dropwise manner and mix by swirling gently. Day 3: Changed to fresh medium; Day 4: Harvest and filter all the culture medium of the 10 cm dish through a 0.45  $\mu$ m filter, pool the filtered media into 729 one bottle. Each 10 cm dish generated approximately 7~8 mL lentivirus crude. Add polybrene 730 731 solution (Sigma-Aldrich) in to the crude virus to a final concentration of 8  $\mu$ g/mL. Aliquot the crude virus into 15 mL tubes (5 mL/tube) and store in -80 °C freezer. 732

733

## 734 Lentivirus titer quantification by flow cytometry (FCM).

735 As the pLenti-TRAP-seq vector expresses a EGFP gene, the functional titer of our lentivirus prep 736 was assayed by FCM as described previously [57]. Briefly, 1) **DAY 1**: split and seed HEK293T cells to 24-well plate,  $5 \times 10^4$  cells per well. Generally, 18 wells were used to perform the titter detection, 737 a gradient volume of the crude lentivirus was added into the cells and each volume was tested by 738 replicates. In this experiment, the crude virus gradients were 2.5  $\mu$ L, 5  $\mu$ L, 10  $\mu$ L, 20  $\mu$ L, 40  $\mu$ L, 80 739 740  $\mu$ L, 160  $\mu$ L and 320  $\mu$ L for each well. Another 2 wells of cells were used for cell counting before transduction; 2) DAY 2: Conduct lentivirus transduction when cells reach up to 60~80% confluence. 741 742 Before transduction, detach the last two wells of cells using 0.05% EDTA-Trypsin to determine the total number of cells in one well (N<sub>(initial)</sub>). Then change the remaining wells with fresh culture 743 744 medium containing 8 µg/mL polybrene, then add the gradient volume of crude virus into each well and swirling gently to mix; 3) **DAY 3**: Change to fresh medium without polybrene; 4) **DAY 4**: Harvest 745 all the cells and wash them twice in PBS. Fix the cells in 4% formalin solution at RT for 20 min, then 746 747 spin down the cell pellet at 2,000 rpm for 5 min. Discard the supernatant and re-suspend the cell pellet Online article

- carefully in 600 μL PBS, and conduct FCM analysis immediately. FCM was performed using a BD
   LSRFortessa<sup>TM</sup> cell analyzer with at least 30,000 events collected for each sample in replicates.
- The FCM output data was analyzed by the software Flowjo vX.0.7. Percentage of GFP-positive cells was calculated as:  $\mathcal{Y}\% = N_{(GFP-positive cells)} / N_{(total cells)} \times 100\%$ . Calculate the GFP percentage of all samples. For accurate titter determination, there should be a linear relationship between the GFP positive percentages and crude volume. The titter (Transducing Units (TU/mL) calculation according to this formula: TU/mL = (N<sub>(initial)</sub> ×  $\mathcal{Y}\% \times 1000$ )/ V. V represents the crude volume ( $\mu$ L) used for initial transduction.
- 757

## 758 Generation of Doxycycline-inducible spCas9/ABE7.10/CBE stable cell lines

TRE-spCas9, TRE-ABE7.10 and TRE-CBE stable cells were generated by PiggyBac transposon 759 760 systems. For stable cell lines establishment, HEK293T cells were transfected with pPB-TRE-spCas9-761 Hygromycin (or pPB-ABE7.10-hygromycin, pPB-CBE-hygromycin) vector and pCMV-hybase with a 9:1 ratio. Briefly,  $1 \times 10^5$  HEK293T cells were seeded in 24-well plate and transfections were 762 conducted 24 h later using lipofectamine 2000 reagent following the manufacturer's instruction. 763 Briefly, 450 ng pPB-TRE-spCas9-Hygromycin (or pPB-ABE7.10-hygromycin, pPB-CBE-764 hygromycin) vectors and 50 ng pCMV-hybase were mixed in 25  $\mu$ L optiMEM (tube A), then 1.5  $\mu$ L 765 lipofectamine 2000 reagent was added in another 25 µL optiMEM and mix gently (tube B). Incubate 766 767 tube A and B at RT for 5 min, then add solution A into B gently and allow the mixture incubating at 768 RT for 15 min. Add the AB mixture into cells evenly in a dropwise manner. Cells transfected with pUC19 were acted as negative control. Culture medium was changed to selection medium with 50 769  $\mu$ g/mL hygromycin 48h after transfection. Completion of selection took approximately 5-7 days until 770 the negative cells were all dead in the un-transfected cells. The cells were allowed to grow in 50 771 772  $\mu$ g/mL hygromycin containing D10 medium for 3-5 days for further expansion. PCR-based genotyping were carry out using the primers: *spCas9-iden-F*: gacacctacgatgatgatctcg; *spCas9-iden*-773 774 R: tggtgctcatcatagcgcttga; ABE7.10-iden-F: 5'-cagtactcgtgctcaacaatcg-3'; ABE7.10-iden-R: 5'-775 ggcgttgcgaacaccgaataca-3'; BE4-iden-F: 5'-ttcttcgatccgagagagctcc-3'; BE4-iden-R: 5'-776 ctgcaccttgtgttcggacag-3'.

777

For functional tests of the spCas9, ABE7.10 and CBE4 expression cells, individual TRAP constructspackaged in lentivirus particles were transduced into the cells. Transduced cells were harvested for

indel analysis 6 days after transduction. Indel analysis were carried out for both the TRAP site andthe endogenous genome target sites.

782

## 783 12K TRAP-seq library lentivirus transduction

HEK293T-SpCas9, -ABE7.10 and -CBE4 cells were cultured in D10 medium with 50 µg/mL 784 hygromycin throughout the whole experiment. For 12K TRAP-seq library transduction, we followed 785 the procedures showed in Fig. S7, S21, S31. Briefly, 1) Day -1:  $2.5 \times 10^6$  cells per 10 cm dish were 786 seeded, and 12 dishes in total. For each group, one dish was used for cell number determination before 787 transduction and one dish for drug-resistance (puromycin) test control and the remaining 10 dishes 788 were used for the 12K TRAP-seq lentivirus library transduction; 2) Day 0: We determined the 789 790 approximate cell number per dish by cell countering. This was used to determine the volume of crude lentivirus used for transduction using a multiplicity of infection (MOI) of 0.3. The low MOI (0.3) 791 792 ensures that most infected cells receive only 1 copy of the lentivirus construct with high probability [34]. The calculation formula is:  $V = N \times 0.3 / TU$ . V = volume of lentivirus crude used for infection 793 (mL); N = cell number in the dish before infection; TU = the titter of lentivirus crude (IFU/mL). In 794 this study, take the TRE-ABE7.10 group for instance, there were  $1.875 \times 10^{-7}$  cells in one dish, the 795 TRAP 12K lentivirus crude titter =  $3.8 \times 10^{6}$  IFU/mL. Thus V =  $1.875 \times 10^{7} \times 0.3 / 3.8 \times 10^{6}$  = 796 1.48 mL. The 12K TRAP-seq transduction coverage per dish is  $1.875 \times 10^{7} \times 0.3 / 12000 = 469 \times 10^{10}$ 797 As we performed 10 replicates for each group, the overall coverage would reach to about  $4690 \times 10^{-10}$  M s 798 799 this study,  $V_{spCas9} = 1.26$  mL,  $V_{ABE7.10} = 1.48$  mL,  $V_{wt} = 1.37$  mL for each dish. For transduction, we added aforementioned volume of crude virus to each group in a dropwise manner and mix by swirling 800 801 gently. The infected cells were cultured in a 37 °C incubator; 3) Day 1: 24 hours after transduction, 802 split the transduced cells of each dish to 3 dishes equally; 4) Day 2: For the 3 dishes of split (30 dishes in total, 3 divided into sub-groups), sub-group 1 (10 dishes) were harvested and labeled as the Day 2 803 804 after 12K TRAP-seq transduction. All cells from this sub-group were pooled into one tube and stored in -20 °C freezer for genomic DNA extraction; The sub-group 2 (10 dishes) was changed to fresh D10 805 medium contains 50  $\mu$ g/mL hygromycin + 1  $\mu$ g/mL puromycin (Dox-free group); The sub-group 3 806 (10 dishes) was changed to D10 medium contains 50  $\mu$ g/mL hygromycin + 1  $\mu$ g/mL puromycin + 1 807  $\mu$ g/mL doxycycline (Dox-induction group). For the WT HEK293T cells (Group 3) screening, 808 809 hygromycin but not puromycin should be excluded from the culture medium; 5) The transduced cells were spitted every 2~3 days when cell confluence reaches up to 90%. At the indicated time points in 810 811 Fig. S7, 21, 31, cells were harvested and stored in -20 °C freezer for further genomic DNA extraction.

812

## 813 PCR amplicons of TRAPs from cells

Genomic DNA was extracted using the phenol-chloroform method. The genomic DNA were digested 814 with RNase A (OMEGA) to remove RNA contamination (In this study, 50  $\mu$ g RNase A worked well 815 to digest the RNA contamination in 100 ~ 200  $\mu$ g genomic DNA after incubating in 37 °C for 30 min). 816 Then the genomic DNA was purified and subjected to PCR for amplification of the TRAP DNA. The 817 PCR primers were: TRAP-NGS-F1: 5'-GGACTATCATATGCTTACCGTA-3' and TRAP-NGS-818 819 R1: 5'-ACTCCTTTCAAGACCTAGCTAG-3'. The PCR product length is 252 bp. In this study, 5  $\mu$ g genomic DNA was used as temperate in one PCR reaction which contained approximately 7.6 × 820  $10^5$  copies of TRAP construct (assuming  $1 \times 10^6$  cells contain 6.6  $\mu$ g genomic DNA), which covered 821 822 about 63 × coverage of the 12K TRAP-seq library. In total, 32 × parallel PCR reactions were 823 performed to achieve approximately  $2.016 \times \text{coverage}$  of each TRAP construct. For each PCR reaction, briefly, 50 µL PCR reaction system consists of 5 µg genomic DNA, 0.5 µL PrimeSTAR 824 825 polymerase, 4 µL dNTP mixture, 10 µL PrimeSTAR buffer, 2.5 µL forward primer (10 uM) and 2.5  $\mu$ L reverse primer (10 uM) and supplemented with ddH2O to a final volume of 50  $\mu$ L. The 826 thermocycle program was 98°C 2min, (98°C for 10s, 55°C for 10s, 72°C for 30s) with 25 cycles, 827 828 then 72°C for 7min and 4°C hold. Then purify all the PCR products by 2% gel, pool the products 829 together and conduct deep amplicon sequencing.

830

## 831 Deep amplicon sequencing

832 MGISEQ-500 (MGI of BGI in China) was used to perform the amplicons deep sequencing following the standard operation protocol. First, PCR-free library was prepared using MGIeasy FS PCR-free 833 DNA library Prep kit following the manufacturer's instruction. Briefly, measure the concentration of 834 purified PCR products using Qubit 4 <sup>TM</sup> fluorometer (Invitrogen) and dilute the concentration of each 835 sample to 10 ng/ $\mu$ L. 10  $\mu$ L diluted PCR product was mixed with an A-Tailing reaction which 836 contained A-Tailing enzyme and buffer, incubated at 37°C for 30 minutes then 65°C for 15 min to 837 838 inactive the enzyme. Then the A-Tailed sample was mixed with PCR Free index adapters (MGI.), T4 839 DNA Ligase and T4 ligase buffer to add index adapter at both 3' and 5' ends of PCR products. The 840 reaction was incubated at 23°C for 30 min and then purified with XP beads. Then denature the PCR products to be single-strand DNA (ssDNA) by incubating at 95 °C for 3 min and keep on 4 °C for the 841 subsequent step. Transform the ssDNA to be circles using cyclase (MGI) at 37 °C for 30 min and 842 843 then digested to remove linear DNA using Exo enzyme at 37 °C for 30 min. Purify the products again

Online article

by XP beads and assay the concentration of library by Qubit 4 <sup>TM</sup> fluorometer. The amplicons libraries were subjected to deep sequencing on the MGISEQ-2000 platform. In this study, for each lane 4 samples (6 ng each) were pooled together for deep sequencing. To avoid sequencing bias induced by base unbalance of TRAP sequence, 12 ng whole-genome DNA library (balance library) was mixed with the 4 PCR samples in a final concentration of 1.5 ng/  $\mu$ L and sequenced in one lane. All the samples were subjected to pair-ended 150 bp deep-sequencing on MGISEQ-500 platform.

850

## 851 Data analysis

852 In order to evaluate the sequencing quality of amplicons and filter the low-quality sequencing data, the default parameters of Fastqc-0.11.3 (http://www.bioinformatics.babraham.ac.uk/projects/fastqc/) 853 854 and fastp-0.19.6 (https://github.com/OpenGene/fastp) were used to carry out the filtration procedure and generate the clean dataset of each sample. The clean sequencing segments of pair-ended TRAP 855 segments were merged using FLASh-1.2.1 (http://ccb.jhu.edu/software/FLASH/index.shtml) to 856 obtain full-length TRAP constructs. The expression characteristics of all the sequences were analyzed 857 by python 3.6, and most of the BsmBI linker fragments changed in orientation (GTTTGGAG-> 858 GTTTGAAT). Therefore, in order to obtain the amplified fragment reads of each TRAP reference 859 860 sequence, the TRAP sequence BsmBI Linker was removed from the reference sequence. The BWA-MEM algorithm of bwa(http://bio-bwa.sourceforge.net/) was used for local alignment, and the reads 861 862 of all samples were divided into 12,000 independent libraries. Due to the existence of sequencing or 863 synthesis introduced errors, each library was then filtered. In order to simplify the filtering process, 864 the filtration strategy varies from TRAP-ABE7.10, TRAP-CBE4.0-gam to TRAP-SpCas9. For ABE7.10 and CBE4.0-gam, they mainly cause single-base variation, rarely introduce insertion and 865 866 deletion, the trap sequence length remains unchanged before and after editing. Therefore, we filter the sequence of each library by locking the intermediate 37bp sequence starting with gRNA + scaffold 867 fragment and ending with GTTT. While TRAP-SpCas9 mainly cause insertion and deletion, the 868 length of trap sequence change around 37bp. Therefore, we adopt three steps to filter the sequence of 869 870 each library. The first step is to obtain the sequence containing gRNA + scaffold fragment as dataset1. 871 The second step is to obtain the sequence containing GTTTGAAT in dataset1 as dataset2. The third 872 step is to extract the intermediate trap sequence from dataset2, which removed the length limit. In order to eliminate the interference of background noise before analyzing editing efficiency, all 873 874 mutations or indels found in WT HEK293T cells group were removed from the Dox group in advance. 875

876	For the TRAP-ABE7.10 and TRAP-CBE4.0-gam, the total editing efficiency for each trap is
877	calculated according to the following formula:
878	Total editing efficiency
879	= ${The \ number \ of \ reads \ whose \ trap \ sequence \ inconsistent \ with \ reference}{The \ total \ reads \ number \ of \ each \ trap}\%$
880	, and the substitution percentage in the 37bp editing window is calculated according to the following
881	formula:
882	Substitution percentage of ABE
883	$= \frac{The \ number \ of \ reads \ with \ actual \ A/T/C/G/N \ base \ in \ specified \ position}{The \ total \ number \ of \ reads \ with \ theoretical \ A \ base \ in \ specified \ position} \%$
884	Substitution percentage of CBE
885	$= \frac{The \ number \ of \ reads \ with \ actual \ A/T/C/G/N \ base \ in \ specified \ position}{The \ total \ number \ of \ reads \ with \ theoretical \ C \ base \ in \ specified \ position} \%$
886	
887	For the TRAP-SpCas9 system, the total editing efficiency for each trap is calculated according to the
888	following formula:
889	Total editing efficiency
890	$= \frac{The \ number \ of \ reads \ whose \ trap \ length \ is \ not \ equal \ to \ 37bp}{The \ total \ reads \ number \ of \ each \ trap}\%$
891	, and the average fraction of indels from 30bp deletion to 10bp insertion is calculated according to
892	the following formula:
893	Average fraction of indels
894	$=\frac{The \ number \ of \ reads \ whose \ trap \ length \ range \ from \ 7-47bp}{The \ total \ reads \ number \ of \ all \ 12k \ trap}\%$
895	
896	Example of selecting low and high efficency gRNA for ABE and CBE. At least one site in this
897	sequence has more than 20% efficient for each TRAP, it is considered that the whole sequence has
898	more than 20% analytical value. Firstly, for the range of N1-N20, divide all TRAP library into a
899	group with an efficiency of greater than 20% and others with an efficiency of 1%, compare the base
900	distribution of the two groups. Then for the range of N5-N7, divide all TRAP library into the above
901	two groups, calculating the base mutation preference of $N-1 \& N + 1$ sites, motif preference and the

902 editing efficiency of N17-N20 sites including GCC, TT and other motif, respectively. For the CBE system, the statistical method is basically the same as that of ABE. Due to the high editing efficiency 903

904 of CBE, in order to correct statistical deviations, CBE divides the efficiency greater than 50% and 905 less than 5% into two groups when calculating the N1-N20 base preference and base mutation 906 preference of N-1 & N+1 site from N4-N8. For the editing window is wider, the efficiency greater 907 than 50% and less than 5% is divided into two groups during the motif preference in N4-N8 window 908 and the editing efficiency of N17-N20 sites including GCC, TT and other motif . Python-3.6 and R 909 scripts were used for efficiency and motif analysis of all the TRAP samples. All visualizations use 910 GraphPad Prism8.2 and R package ggplot2.

911

## 912 GNL machine learning featurization

The feature set applied in our model construction contains 2485 features, which includes following 913 five categories. (i) 604 features of "one-hot" encoding of the nucleotide. There are two subsets in this 914 915 category: position-dependent and position-independent. And each category applies to the one nucleotide and pairwise nucleotide. Such as " nuc pd Order2" consisted of e.g. AA 1/AT 1/AG 1, 916 and "nuc pd Order1" consisted of e.g. A 1/T 1/G 1/C 1. (ii) 3 GC features, which consists of GC 917 count, GC count < 10, GC count > 10. (iii) 16 features of the two nucleotides flanking the NGG PAM 918 919 in the 5' and 3'. (iv) Five thermodynamic features. We calculated five thermodynamic features ausing the "Tm staluc function" in Biopython package. All these features above were derived from the 920 921 30mer of target sequences. (v) 1856 features of three nucleotides with "position-dependent" and 922 "position-independent", such as ACG/AGG and ACG 1/ACT 2. Note that, all these features were 923 encoded by 30mer context sequence.(vi) Free energy (DeltaG), which was calculated by the local 924 version of "mfold" (http://unafold.rna.albany.edu/?q=mfold/download-mfold). We used the binary 925 programme "quikfold" in the same bin file of "mfold" to calculate multiple input sequences in the 926 same time. All the parameters were set as default, to make sure the outputs of each 20mer sequences 927 be the same as the webpage.

928

## 929 Model training: Comparison with other machine learning models

We trained model to predict the cleavage efficiency of each site in the editing windows among ABE and CBE editing system. For the whole sequence sites of gRNA, three type of editing system was uniformly trained by the same BRR model. To select the optimized predictive model, we initially compared the predictive performance among eight models, they are, Bayesian Ridge regression (BRR), gradient boosted regression tree (GBRT), decision tree (DT), L1-regression (L1-reg), L2regression (L2-reg), linear regression (LR), neural network (NN), random forest (RF). All these

algorithms were trained under the same features vector spaces. The mean performance of each algorithm was conducted by 10-fold cross validation. Because all of them can be used as regression, the performance was evaluated by SCC (Spearman Correlation coefficient). The model with best performance, highest SCC value and lowest S.D., was selected. Finally, BRR was outperform than other counterparts. All the models applied for training using the scikit-learn package in python. During training, optimal hyper-parameter was chose using the inner 10-fold cross validation, using the grid search. After that,  $\alpha$  and  $\lambda$  were both set as 1.e-6.

943

## 944 Bayesian Ridge Regression

945 Bayesian Ridge regression is changed from Bayesian linear regression by adding the prior of 946 coefficient " $\omega$ " as spherical Gaussian and the priors over lambda are chosen to be gamma distributions, 947 which is similar to the classical Ridge regression [58]. Bayesian linear regression is briefly shown as 948 (1), and the coefficients of w is hypothesized as the spherical distribution to find a maximum 949 posteriori estimation of  $\omega$  as (2) shows.

$$P(y|X, \omega, \alpha) = N(y|X\omega, \alpha)$$
(1)

950 Where  $\alpha$  is treated as a random variable that is to be estimated from the data as gamma distribution. 951

$$\mathbf{P}(\boldsymbol{\omega}|\boldsymbol{\lambda}) = \mathbf{N}(\boldsymbol{\omega}|\boldsymbol{0},\boldsymbol{\lambda}^{-1}\boldsymbol{I}_{p}) \tag{2}$$

953 Where  $\lambda$  is also treated as a random variable that is to be estimated from the data, and also be 954 hypothesized as gamma distribution.

955

952

## 956 Model explanation

957 In addition to train the model with high performance, we also interested in the model importance for 958 our final model. We used SHAP (SHapley Additive exPlanations) algorithm [59], which is a 959 unified approach to explain the output of any machine learning model. Importantly, we excluded the 960 necessary site when training the site model for each editing system. E.g. We drop A1 when training 961 the N1 site of ABE system. So, the importance of the left features can be ranked by the SHAP value, 962 and the top 20 important features of each model were shown for each editor.

963

## 964 DATA AVAILABILITY

- 965 NGS data: CNBG accession number: TBD
- 966 Code for machine learning: <u>https://github.com/TerminatorJ/CRISPR-TRAP-seq.git</u>
- 967 CRISPR atlas: <u>www.crispratlas.com/crispr</u>
- 968

## 969 ACKNOWLEDGEMENT

This project is supported by the Sanming Project of Medicine in Shenzhen (SZSM201612074), 970 971 Qingdao-Europe Advanced Institute for Life Sciences Grant, Guangdong Provincial Key Laboratory 972 of Genome Read and Write (No. 2017B030301011) and Guangdong Provincial Academician Workstation of BGI Synthetic Genomics (No. 2017B090904014) . Y.L. is supported by BGI-973 Research and Brainstem Center of Excellence (Danish Innovation Fund, BrainStem). L.L. is 974 975 supported by the Lundbeck Foundation (R219–2016-1375) and the DFF Sapere Aude Starting grant (8048-00072A). G.C. is supported by National Human Genome Research Institute of the National 976 977 Institutes of Health [RM1HG008525]. We thank the China National GeneBank for the support of 978 executing the project under the framework of Genome Read and Write.

979

## 980 AUTHOR CONTRIBUTION

981 L.L. and Y.L. conceived the idea. L.B, G.C, L.L and Y.L oversaw the whole study. X.X, K.Q, L.L.

- and Y.L. and designed the study. X.X, K.Q, X.L, and X.P performed most of the experiments and
- analyses. All authors have contributed to the execution of the experiments and studies. L.L. and Y.L.
- 984 drafted the manuscript. All authors discussed the results and contributed to the final manuscript.
- 985

## 986 CONFLICT OF INTEREST

987 The authors declare no conflict of interest.

988

## 989 **REFERENCEs**

- Mali, P., et al., *RNA-guided human genome engineering via Cas9*. Science, 2013. **339**(6121):
   p. 823-6.
- 2. Cong, L., et al., *Multiplex genome engineering using CRISPR/Cas systems*. Science, 2013.
   339(6121): p. 819-23.
- Jinek, M., et al., A programmable dual-RNA-guided DNA endonuclease in adaptive bacterial
   *immunity.* Science, 2012. **337**(6096): p. 816-21.
- 996 4. Farboud, B., et al., Enhanced Genome Editing with Cas9 Ribonucleoprotein in Diverse Cells
  997 and Organisms. J Vis Exp, 2018(135).
- 9985.Hwang, W.Y., et al., Efficient genome editing in zebrafish using a CRISPR-Cas system. Nat999Biotechnol, 2013. **31**(3): p. 227-9.

- Friedland, A.E., et al., *Characterization of Staphylococcus aureus Cas9: a smaller Cas9 for all- in-one adeno-associated virus delivery and paired nickase applications.* Genome Biol, 2015.
   **16**: p. 257.
- 10037.Muller, M., et al., Streptococcus thermophilus CRISPR-Cas9 Systems Enable Specific Editing1004of the Human Genome. Mol Ther, 2016. 24(3): p. 636-44.
- 10058.Hou, Z., et al., Efficient genome engineering in human pluripotent stem cells using Cas9 from1006Neisseria meningitidis. Proc Natl Acad Sci U S A, 2013. **110**(39): p. 15644-9.
- 10079.Kleinstiver, B.P., et al., Broadening the targeting range of Staphylococcus aureus CRISPR-1008Cas9 by modifying PAM recognition. Nat Biotechnol, 2015. **33**(12): p. 1293-1298.
- 1009 10. Zetsche, B., et al., *Cpf1 is a single RNA-guided endonuclease of a class 2 CRISPR-Cas system.*1010 Cell, 2015. **163**(3): p. 759-71.
- 1011 11. Cox, D.B.T., et al., *RNA editing with CRISPR-Cas13*. Science, 2017. **358**(6366): p. 1019-1027.
- 1012 12. Yeh, C.D., C.D. Richardson, and J.E. Corn, *Advances in genome editing through control of DNA* 1013 *repair pathways.* Nat Cell Biol, 2019. **21**(12): p. 1468-1478.
- 101413.Qi, L.S., et al., Repurposing CRISPR as an RNA-guided platform for sequence-specific control1015of gene expression. Cell, 2013. **152**(5): p. 1173-83.
- 101614.Lin, L., et al., Genome-wide determination of on-target and off-target characteristics for RNA-1017guided DNA methylation by dCas9 methyltransferases. Gigascience, 2018. 7(3): p. 1-19.
- 101815.Chen, B., J. Guan, and B. Huang, Imaging Specific Genomic DNA in Living Cells. Annu Rev1019Biophys, 2016. 45: p. 1-23.
- 102016.Kang, B.C., et al., Precision genome engineering through adenine base editing in plants. Nat1021Plants, 2018. 4(7): p. 427-431.
- 102217.Zong, Y., et al., Precise base editing in rice, wheat and maize with a Cas9-cytidine deaminase1023fusion. Nat Biotechnol, 2017. **35**(5): p. 438-440.
- 102418.Komor, A.C., et al., Programmable editing of a target base in genomic DNA without double-1025stranded DNA cleavage. Nature, 2016. **533**(7603): p. 420-4.
- 102619.Gaudelli, N.M., et al., Programmable base editing of A\*T to G\*C in genomic DNA without1027DNA cleavage. Nature, 2017. 551(7681): p. 464-471.
- 102820.Koblan, L.W., et al., Improving cytidine and adenine base editors by expression optimization1029and ancestral reconstruction. Nat Biotechnol, 2018. **36**(9): p. 843-846.
- 103021.Rees, H.A., et al., Improving the DNA specificity and applicability of base editing through1031protein engineering and protein delivery. Nat Commun, 2017. 8: p. 15790.
- 103222.Nishida, K., et al., Targeted nucleotide editing using hybrid prokaryotic and vertebrate1033adaptive immune systems. Science, 2016. **353**(6305).
- 103423.Zhang, Y., et al., Programmable base editing of zebrafish genome using a modified CRISPR-1035Cas9 system. Nat Commun, 2017. 8(1): p. 118.
- 103624.Jensen, K.T., et al., Chromatin accessibility and guide sequence secondary structure affect1037CRISPR-Cas9 gene editing efficiency. FEBS Lett, 2017. 591(13): p. 1892-1901.
- 103825.Uusi-Makela, M.I.E., et al., Chromatin accessibility is associated with CRISPR-Cas9 efficiency1039in the zebrafish (Danio rerio). PLoS One, 2018. **13**(4): p. e0196238.
- 1040 26. Kim, H.K., et al., *High-throughput analysis of the activities of xCas9, SpCas9-NG and SpCas9*1041 *at matched and mismatched target sequences in human cells.* Nat Biomed Eng, 2020. 4(1):
  1042 p. 111-124.
- 104327.Shen, M.W., et al., Predictable and precise template-free CRISPR editing of pathogenic1044variants. Nature, 2018. 563(7733): p. 646-651.

- 104528.Allen, F., et al., Predicting the mutations generated by repair of Cas9-induced double-strand1046breaks. Nat Biotechnol, 2018.
- 104729.Zhou, Y., et al., Enhanced genome editing in mammalian cells with a modified dual-1048fluorescent surrogate system. Cell Mol Life Sci, 2016. **73**(13): p. 2543-63.
- 1049 30. Komor, A.C., et al., *Improved base excision repair inhibition and bacteriophage Mu Gam* 1050 *protein yields C:G-to-T:A base editors with higher efficiency and product purity.* Sci Adv, 2017.
   1051 **3**(8): p. eaao4774.
- Sjostedt, E., et al., *An atlas of the protein-coding genes in the human, pig, and mouse brain.*Science, 2020. **367**(6482).
- 105432.Billon, P., et al., CRISPR-Mediated Base Editing Enables Efficient Disruption of Eukaryotic1055Genes through Induction of STOP Codons. Mol Cell, 2017. 67(6): p. 1068-1079 e4.
- 105633.Xu, Y., et al., A new massively parallel nanoball sequencing platform for whole exome1057research. BMC Bioinformatics, 2019. **20**(1): p. 153.
- 1058 34. Shalem, O., et al., *Genome-scale CRISPR-Cas9 knockout screening in human cells.* Science,
  1059 2014. 343(6166): p. 84-87.
- 106035.Morgens, D.W., et al., Genome-scale measurement of off-target activity using Cas9 toxicity1061in high-throughput screens. Nat Commun, 2017. 8: p. 15178.
- 106236.Tycko, J., V.E. Myer, and P.D. Hsu, Methods for Optimizing CRISPR-Cas9 Genome Editing1063Specificity. Mol Cell, 2016. 63(3): p. 355-70.
- 106437.Kosicki, M., et al., Dynamics of Indel Profiles Induced by Various CRISPR/Cas9 Delivery1065Methods. Prog Mol Biol Transl Sci, 2017. 152: p. 49-67.
- 1066 38. Lin, L. and Y. Luo, *Tracking CRISPR's Footprints*. Methods Mol Biol, 2019. **1961**: p. 13-28.
- 106739.Moller, H.D., et al., CRISPR-C: circularization of genes and chromosome by CRISPR in human1068cells. Nucleic Acids Res, 2018. 46(22): p. e131.
- 106940.Wang, D., et al., Optimized CRISPR guide RNA design for two high-fidelity Cas9 variants by1070deep learning. Nat Commun, 2019. **10**(1): p. 4284.
- 1071 41. Graf, R., et al., sgRNA Sequence Motifs Blocking Efficient CRISPR/Cas9-Mediated Gene Editing.
  1072 Cell Rep, 2019. 26(5): p. 1098-1103 e3.
- 107342.Ata, H., et al., Robust activation of microhomology-mediated end joining for precision gene1074editing applications. PLoS Genet, 2018. 14(9): p. e1007652.
- 107543.Wang, J., et al., GNL-Scorer: A generalized model for predicting CRISPR on-target activity by1076machine learning and featurization. J Mol Cell Biol, 2020.
- 107744.Concordet, J.P. and M. Haeussler, CRISPOR: intuitive guide selection for CRISPR/Cas9 genome1078editing experiments and screens. Nucleic Acids Res, 2018. 46(W1): p. W242-W245.
- 107945.Xue, L., et al., Prediction of CRISPR sgRNA Activity Using a Deep Convolutional Neural1080Network. J Chem Inf Model, 2019. 59(1): p. 615-624.
- 108146.Labuhn, M., et al., Refined sgRNA efficacy prediction improves large- and small-scale CRISPR-1082Cas9 applications. Nucleic Acids Res, 2018. 46(3): p. 1375-1385.
- 108347.Hwang, G.H., et al., Web-based design and analysis tools for CRISPR base editing. BMC1084Bioinformatics, 2018. 19(1): p. 542.
- 108548.Dandage, R., et al., beditor: A Computational Workflow for Designing Libraries of Guide RNAs1086for CRISPR-Mediated Base Editing. Genetics, 2019. 212(2): p. 377-385.
- 108749.Ramakrishna, S., et al., Surrogate reporter-based enrichment of cells containing RNA-guided1088Cas9 nuclease-induced mutations. Nat Commun, 2014. 5: p. 3378.

- 1089 50. Kim, H., et al., Surrogate reporters for enrichment of cells with nuclease-induced mutations.
  1090 Nat Methods, 2011. 8(11): p. 941-3.
- 109151.Cullot, G., et al., CRISPR-Cas9 genome editing induces megabase-scale chromosomal1092truncations. Nat Commun, 2019. 10(1): p. 1136.
- 1093 52. Kosicki, M., K. Tomberg, and A. Bradley, *Repair of double-strand breaks induced by CRISPR-*1094 *Cas9 leads to large deletions and complex rearrangements.* Nat Biotechnol, 2018. **36**(8): p.
  1095 765-771.
- 1096 53. Hu, J.H., et al., *Evolved Cas9 variants with broad PAM compatibility and high DNA specificity.*1097 Nature, 2018. **556**(7699): p. 57-63.
- 109854.Slaymaker, I.M., et al., Rationally engineered Cas9 nucleases with improved specificity.1099Science, 2016. **351**(6268): p. 84-8.
- 110055.Kleinstiver, B.P., et al., High-fidelity CRISPR-Cas9 nucleases with no detectable genome-wide1101off-target effects. Nature, 2016. 529(7587): p. 490-5.
- 110256.Kuscu, C., et al., CRISPR-STOP: gene silencing through base-editing-induced nonsense1103mutations. Nat Methods, 2017. 14(7): p. 710-712.
- 110457.Kutner, R.H., X.Y. Zhang, and J. Reiser, Production, concentration and titration of1105pseudotyped HIV-1-based lentiviral vectors. Nat Protoc, 2009. 4(4): p. 495-505.
- 110658.Tipping, M.E., Sparse Bayesian learning and the relevance vector machine. Journal of1107machine learning research, 2001. 1(Jun): p. 211-244.
- 1108 59. Lundberg, S.M. and S.-I. Lee. *A unified approach to interpreting model predictions*. 2017.
- 1109 1110